

**Ohio Water Resources Center
Annual Technical Report
FY 2012**

Introduction

Pursuant to the Water Resources Research Act of 1964, the Ohio Water Resources Center (Ohio WRC) is the federally-authorized and state-designated Water Resources Research Institute (WRRI) for the State of Ohio.

The Ohio WRC was originally established in 1959 as part of the Engineering Experiment Station, College of Engineering, OSU, and conducted an extensive program of research on water and wastewater treatment processes. The Center continues to be administered through the College of Engineering and has maintained a tradition of placing special emphasis on encouraging and supporting research in the area of physical, chemical, and biological treatment processes for water and wastewater. The mission of Ohio WRC is to promote innovative, water-related research in the State of Ohio through research grant competitions, coordination of interdisciplinary research proposals, and educational outreach activities.

Research Program Introduction

Over this past year's reporting period we sponsored five new research projects conducted at four different Ohio universities totaling \$686,663 in research funding (direct and cost share). Fifteen students majoring in environmental engineering, civil engineering, chemical engineering, environmental science, biology and other water related fields were supported on these projects. Four journal articles were published, with more under development and/or under review. Nineteen conference presentations were made during this report period.

The funded research projects entail studies of important Ohio Water Resources problems. For example, Dr. Paula Mouser investigated wetland function in nitrogen cycling and methane emission. Some projects were not yet finalized and will be ongoing in the next year, such as Dr. John Senko's investigation of microbial modulation of acidic coal mine drainage activity for minewater treatment, and Dr. Xiaozhen Mou's research on the identification of microcystin-degrading bacteria in the Grand Lake St. Marys and Lake Erie Western Basin. Although progressing, Dr. John Lenhart's research to discriminate biotic and abiotic arsenic release processes under highly reduced groundwater will also continue next year.

The Constructed Wetland Dilemma: Nitrogen Removal at the Expense of Methane Generation?

Basic Information

Title:	The Constructed Wetland Dilemma: Nitrogen Removal at the Expense of Methane Generation?
Project Number:	2011OH205B
Start Date:	3/1/2011
End Date:	8/31/2013
Funding Source:	104B
Congressional District:	OH-12
Research Category:	Engineering
Focus Category:	Nitrate Contamination, Wetlands, Ecology
Descriptors:	
Principal Investigators:	Paula J Mouser, Gil Bohrer

Publications

1. Mouser, Paula, Michael Brooker, William Mitsch, Gil Bohrer, 2012, Factors Influencing Microbial Gas Production Rates in a Constructed Wetland Ecosystem. Oral Presentation, 5/2012, In 30th AMS Conference on Agricultural and Forest Meteorology, Boston, MA.
2. Bohrer, Gil; Liel Naor-Azrieli; Scott Mesi; Paula Mouser; K Stefanik; KV Schafer; William Mitsch, 2012, Determining the meteorological forcing that affect seasonal and diurnal dynamics of methane emissions at a constructed urban wetland in Ohio. Oral Presentation, 5/2012, In 30th AMS Conference on Agricultural and Forest Meteorology, Boston, MA.
3. Shafer, KV; Gil Bohrer, Liel Naor-Azrieli, Paula Mouser, William Mitch, M Wu, 2011, Temporal Dynamics of Methane Fluxes in Temperate Urban Wetlands, Poster Presentation B12C-05, 12/2011, In American Geophysical Annual Meeting, San Francisco, CA.
4. Naor-Azrieli, Liel; Gil Bohrer, William Mitsch, 2011, Collaborative research: Greenhouse gas balance of urban temperate wetlands. Oral presentation, 5/2011, In Annual Meeting of the American Ecological Engineering Society, Ashville, NC.
5. Mouser, PJ, Brooker, M, Bohrer, G. (2012), Factors Influencing Microbial Gas Production Rates in Wetland Sediments. Oral Presentation, 10/2012. 4th International EcoSummit Ecological Sustainability: Restoring the Planet's Ecosystem Services, Columbus, OH.
6. Brooker, M, Mitsch, W, Bohrer, G, Mouser, PJ. (2012), Factors Influencing Methane Emission Potential from Wetland Sediments. Oral Presentation, 6/2012. 2012 Ohio River Basin Consortium for Research and Education Symposium, Athens, OH.
7. Brooker, M., Bohrer, G., Mouser, P.J. (2012) Factors Influencing Microbial Carbon Emission Potential from Wetland Sediments and its Relation to Surface- and Plot-Scale Measurements, B33C-0536, poster presentation at Fall Meeting, AGU, San Francisco, Calif., 3-7 Dec.

Progress Report 2012-2013

Contract Information

Title	The Constructed Wetland Dilemma: Nitrogen Removal at the Expense of Methane Generation?
Project Number	2011OH205B
Start Date	3/1/2011
End Date	2/28/2013
Focus Category	Nitrate Contamination, Wetlands, Ecology
Keywords	Bacteria, Biotechnology, Nitrate Removal, Methane Flux, Constructed Wetlands
Lead Institute	The Ohio State University
Principal Investigators	Paula Mouser, Gil Bohrer

Abstract

Constructed wetlands provide a valuable ecosystem service by sequestering carbon dioxide from the atmosphere and serving as a sink for atmospheric nitrogen export. Unfortunately, carbon sequestration and denitrification in wetlands come with the tradeoff of increased production of methane – another more potent green house gas. Methane is produced by methanogenic archaea that thrive in chemically reduced, anaerobic zones of the wetland. Dinitrogen export, on the other hand, is thought to occur under suboxic conditions by denitrifying bacteria. Few studies have examined the *in situ* rates of metabolic activity for dominant microorganisms driving these processes or systematically evaluated the key factors controlling their metabolic rates in wetland environments. This research evaluates how three environmental factors: temperature, wetland biome, and redox environment relate to microbial ecology and *in situ* gas production in a constructed wetland ecosystem located in central Ohio. Microbial measurements provide information about instantaneous fluxes under differing environmental conditions but are not necessarily representative of long-term fluxes that may be quantified using surface chamber measurements or atmospheric eddy-covariance methods. The objective of this research is to develop upper limit estimates for *in situ* microbial gas production rates under differing environmental conditions so that we may better understand how they relate to spatiotemporal surface and plot-scale emission rates also measured at the site.

Problem

Sources of fixed nitrogen (N) are essential for the growth of all biological organisms, and agriculture is dependent on nitrogen supply for fertilization. When present at elevated levels in drinking water, however, certain nitrogen species present significant health risks to humans including blue baby syndrome, enlarged thyroids, and increased risk of certain cancers. It can also contribute to hypoxic conditions in certain lakes and coastal environments. For example, eutrophication in the Gulf of Mexico and the Great Lakes region has largely been attributed to imbalances between nitrogen fertilizer application and crop uptake, and precipitation runoff from livestock feed lots in Ohio and other mid-West states. Limiting the transport of nitrogen from its source is therefore critical to protecting Ohio's water resources and lowering health risks and environmental impacts to nearby regions.

One suggested method for reducing nitrogen export is the use of constructed wetlands or riparian buffer zones between discharge points and water bodies to transform aquatic anthropogenic N inputs, such as nitrate, to a gaseous form released to the atmosphere, thereby reducing its transport to potential receptors. Unfortunately, denitrification in wetlands comes with the tradeoff of increased Green House Gas (GHG) production. In order to allow development of wetlands as a solution for N removal without concerns of GHG production, it is critical to understand what factors control methane production and how emissions relate to wetland aquatic conditions.

A preliminary study using microcosms were used to estimate the maximum potential flux of greenhouse gases from wetland sediments under controlled laboratory conditions. Despite temperature being a known factor on microbial activity, carbon flux potentials were not found to be significantly impacted by a change of temperature from 20°C to 30°C. The location of the sediment was found to impact the rate of methane production. The lack of statistical significance with relationship to temperature was caused by large variations and thus a more comprehensive study was designed to investigate other possible factors involved in the GHG production. **The objectives of this research are to: 1) link environmental conditions such as site location, temperature, and nutrient availability to GHG emissions 2) investigate differences in microbial community as it pertains to GHG emissions and N budgets.** Progress to date on these objectives includes the following methods and findings.

Methodology

Between June and December 2012, we performed laboratory experiments to understand the factors that influence methanogenesis and denitrification at the ORWRP. Sediment cores were collected from distinct biomes and split by depth. These included the shallow (SH, top 15 cm) and deep (DE, bottom 15 cm) locations from 30 cm cores collected from an inundated, open water site (OW) and an edge zone with vegetation (VEG). An automated on-line monitoring setup at the wetland measures soil temperature and carbon-based GHG emissions with use of a meteorological station at the wetland site. Microcosms were constructed in 150 ml serum bottles with sediment (25 g) and water collected from the inlet pipe (75 ml). Samples were gassed under 80:20% N₂:CO₂ to produce anaerobic conditions, then incubated at two temperatures (20°C or 30°C) over the course of 77 days. Triplicates were prepared concurrently for use in water-quality and headspace gas analysis. Headspace gas samples were taken periodically from each set and analyzed on a Shimadzu GC-14A. The triplicates were sacrificed at these sampling points and water was filtered and analyzed for anion presence using the Dionex ICS-2100 and dissolved organic carbon using the Shimadzu TOC-V CSN systems. An amendment study using enrichment of two potential methanogenic substrates - acetate or carbon dioxide – utilized triplicate microcosms for each temperature from the OW-DE sediments for headspace gas analysis.

Samples of the initial sediments were taken upon return to the laboratory and stored at -80°C. Sediment (~0.5 g) was thawed and used in the isolation of genomic DNA present using the MoBio PowerSoil DNA extraction kit as per the manufacturer's directions. A universal 16S rRNA primer set (515F-806R) with barcode-primers was used to amplify the samples and analysis was performed with a Roche 454-sequencing apparatus. Sequencing results were processed through the QIIME virtual pipeline.

Results

Depth was found to be a major factor in methane flux potentials from the biomes with almost no methane production observed in the deeper sediments. Across the two shallow zones, a near doubling in methane flux potential was found to be statistically significant in relationship to the higher temperature (Figure 1). Although a higher potential flux rate was observed within the 30°C treatment for the OW-SH compared to the VEG-SH site it was not statistically significant across the site. Carbon dioxide potential flux rates were also found to double with the higher temperature across this experiment. Depth was found to have a significant effect on gas production, with DE sites showing lower rates than corresponding SH sediments. Acetate was found to significantly stimulate methanogenesis in the OW-DE sediments. No methanogenic production was observed in the carbon dioxide-amended samples (Figure 1).

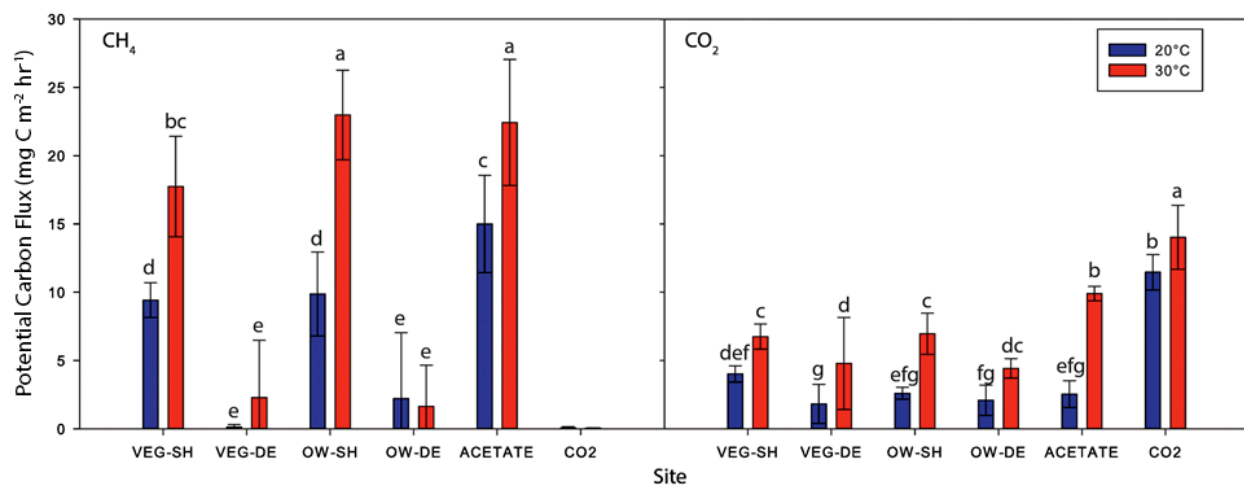


Figure 1. Methane and carbon dioxide flux potentials calculated from the four biomes and amendments at each temperature. Letters represent levels of statistical differences between each set.

Nitrogen, in the form of nitrate and nitrite, were not found at considerable levels for the majority of the experiment and showed no discernable trends (Figure 2). Sulfate was a significant indicator for the lack of methane production from the deep sediments. Considered the final electron acceptor which limits methanogenesis, sulfate was found to decrease to the detection limit in the SH sediments by day 21 corresponding to the stabilization of methanogenic production rates in those samples. However, very limited sulfate reduction was noticed in the DE samples across the 77 day experiment (Figure 2).

Microbial communities were found to be different among the four biomes. The greatest similarity was found to be based upon biome (OW vs VEG). The OW site was found to have the highest relative abundance of methanogens at 4.5% and 4.8% for the SH and DE depths, respectively. The VEG-SH site was found to have a lower relative abundance of 1.5%, while the VEG-DE site had the lowest at 0.1%. The two classes of methanogens are *Methanomicrobia* and *Methanobacteriales*. The *Clostridia* and *Deltaproteobacteria* constitute some acetogens and syntrophs, both of which can provide methanogens with necessary substrates. Some *Betaproteobacteria* are known to be denitrifiers while *Gammaproteobacteria* and *Alphaproteobacteria* are known to have organisms capable of denitrification as well as

methanotrophy. *Mehtylacidiphilae*, a class of the *Verrucomicrobia* is also related to methanotrophy. There is recent evidence that suggest the NC10 phyla to actually link the process of denitrification directly to methane oxidation resulting in the flux of N₂ and CO₂ gas. Figure 3 shows the relative abundances of these groups of organisms.

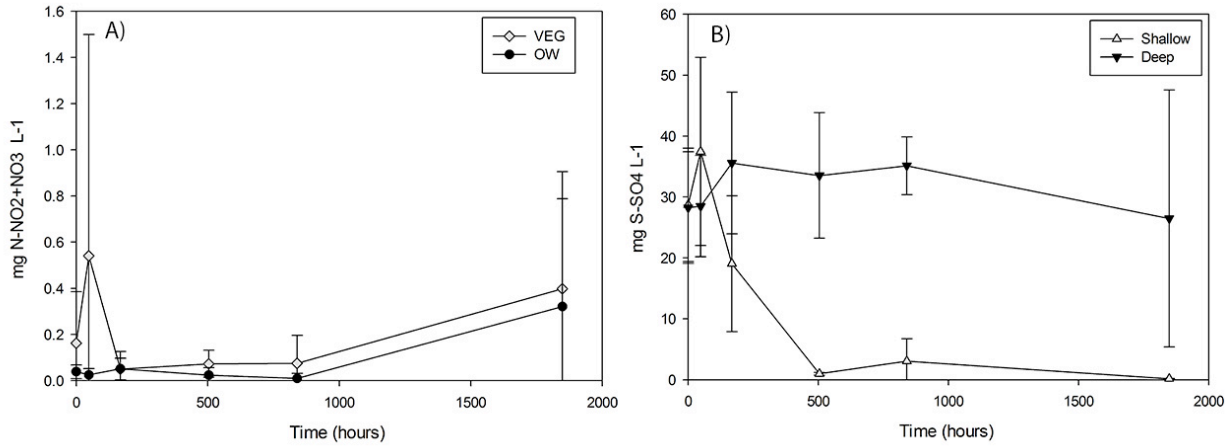


Figure 2. A) Observed nitrogen concentration based upon site. B) Observed sulfate concentration based upon depth.

While the OW sites show a higher abundance of methanogens compared to the VEG sites, the VEG-SH site shows the greatest abundance of the organisms that would typically be thought of as providing environmental benefits. The VEG-DE site had a lower abundance of these organisms, but also contained the least amount of the organisms that can be responsible for methane. The VEG sites were found to have the greatest amounts of nitrogen oxidizing organisms. Further data reduction is underway to link pyrosequencing data to biogeochemical trends.

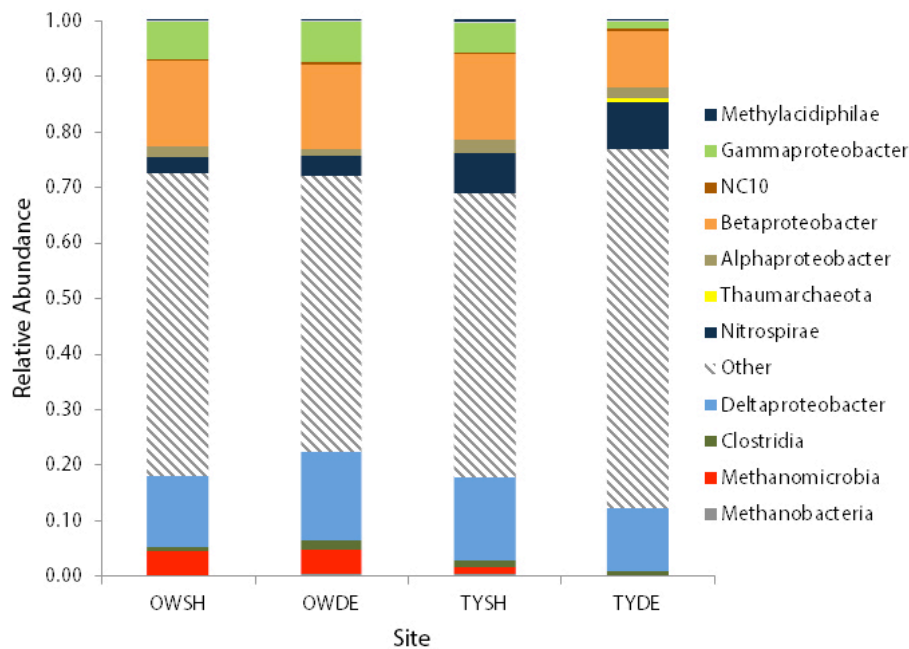


Figure 3. Relative abundance of key microorganisms involved in nitrogen or methane cycling from wetland sediments. Top illustrates organisms thought of as benefiting water quality or methanotrophy, and bottom illustrates organisms involved in methane production.

Significance

Our findings suggest that temperature impacts the methane flux potential of wetland sediments by enhancing microbial activity. Location seems to impact methane flux potential at these higher temperatures while the effect is not present at lower temperatures. Deeper sediments appear to lack something that allows for methanogenesis to occur, whether it is a form of carbon or a microorganism not present in the community capable of providing methanogens' their substrates. The prevalence of methanogens at the OW site and lower abundance in VEG site suggest that this area can have a larger impact on methane production, while the number of possible methane oxidizers and nitrogen-cyclers indicate these areas may provide more of the wetland benefits. It is evident that microbial communities show differences based upon the wetland biomes and may serve to indicate the functional potentials these zones have in influencing wetland biogeochemical cycling.

The results of this paper are currently being developed into a thesis for M. Brooker to be defended in July 2013. Mike is also preparing a manuscript from this research, with an expected submission date of August 2013.

Publications/Proceedings/Conference Presentations

1. Mouser, PJ, Brooker, M, Bohrer, G. (2012), Factors Influencing Microbial Gas Production Rates in Wetland Sediments. Oral Presentation, 10/2012. *4th International EcoSummit Ecological Sustainability: Restoring the Planet's Ecosystem Services, Columbus, OH.*
2. Brooker, M, Bohrer, G, Mouser, PJ. (2012), Quantifying *in situ* Rates of Methanogenesis and Denitrification from Wetland Sediments. Poster Presentation, 10/2012. *4th International EcoSummit Ecological Sustainability: Restoring the Planet's Ecosystem Services, Columbus, OH.*
3. Brooker, M, Mitsch, W, Bohrer, G, Mouser, PJ. (2012), Factors Influencing Methane Emission Potential from Wetland Sediments. Oral Presentation, 6/2012. *2012 Ohio River Basin Consortium for Research and Education Symposium, Athens, OH.*
4. Brooker, M., Bohrer, G., Mouser, P.J. (2012) Factors Influencing Microbial Carbon Emission Potential from Wetland Sediments and its Relation to Surface- and Plot-Scale Measurements, B33C-0536, poster presentation at *Fall Meeting, AGU, San Francisco, Calif., 3-7 Dec.*
5. Mouser, PJ, Brooker, M, Mitsch, W, and Bohrer, G. (2012), Factors Influencing Microbial Gas Production Rates in a Constructed Wetland Ecosystem. Oral Presentation, 5/2012. *30th AMS Conference on Agricultural and Forest Meteorology, Boston, MA.*
6. Bohrer, G, Naor-Azieli, L, Mesi, S, Mouser, PJ, Stefanik, K, Schafer, KVR, and Mitsch, W (2012), Determining the meteorological forcing that affect seasonal and diurnal dynamics of methane emissions at a constructed urban wetland in Ohio. Oral Presentation, 5/2012. *30th AMS Conference on Agricultural and Forest Meteorology, Boston, MA.*

7. Shafer, KV, Bohrer, G, Naor, L, Mouser, PJ, Mitsch, WJ, Wu, M (2011), Temporal Dynamics of Methane Fluxes in Temperate Urban Wetlands, Poster Presentation B12C-05, 12/2011. *American Geophysical Annual Meeting, San Francisco, CA.*

8. Naor-Azrieli, L, Bohrer G, Mitsch W. (2011), Collaborative research: Greenhouse gas balance of urban temperate wetlands. Oral presentation 5/2011. *Annual Meeting of the American Ecological Engineering Society, Ashville, NC.*

Students Supported By Project

1. Michael Brooker – M.S. student in Environmental Science Graduate Program (June 2011-May 2013).

Awards or Achievements

None to date.

Generating Renewable Energy on Lake Erie with Wave Energy Converters: A Feasibility Study

Basic Information

Title:	Generating Renewable Energy on Lake Erie with Wave Energy Converters: A Feasibility Study
Project Number:	2011OH239B
Start Date:	3/1/2011
End Date:	2/28/2014
Funding Source:	104B
Congressional District:	15
Research Category:	Engineering
Focus Category:	Models, Surface Water, Water Quality
Descriptors:	
Principal Investigators:	Ethan John Kubatko, Ethan John Kubatko

Publications

1. Dibling, Dave; Ethan Kubatko, Generating Renewable Energy on Lake Erie with wave energy converters: a feasibility study, Great Lakes Research, in preparation.
2. Kubatko, Ethan, 2011, Development of a high-resolution, nearshore model for Lake Erie, The 10th International Workshop on Multiscale (Un-)structured Mesh Numerical Modelling for coastal, shelf and global ocean dynamics, August 2011.
3. Kubatko, Ethan, 2012, Validation of a high-resolution finite element model for Lake Erie, In World Congress on Computational Mechanics, July 2012.
4. Kubatko, Ethan, 2013, Introducing DG-Wave: A discontinuous Galerkin-based wave prediction model, The ADCIRC Annual Workshop, April 2013.
5. Kubatko, Ethan, 2013, Development and Validation of DG-Wave, US National Congress on Computational Mechanics.

GENERATING RENEWABLE ENERGY ON LAKE ERIE WITH WAVE ENERGY CONVERTERS: A FEASIBILITY STUDY

Principal Investigator:

Ethan J. Kubatko, Assistant Professor
Department of Civil & Environmental Engineering & Geodetic Science
The Ohio State University

1 Research Objectives

The primary objective of this research is to investigate the feasibility of generating clean, renewable energy on Lake Erie by harnessing the Lake's wave energy through the use of a novel kinetic energy harvesting technology called nPower[®] developed by Tremont Electric, LLC, a Cleveland-based alternative energy company. Specifically, feasibility of this idea will be investigated by performing wave energy simulations that make use of two critical modeling components described in detail below: 1) a *high-resolution, unstructured mesh* of Lake Erie that provides highly accurate measurements of the bathymetry and the shoreline of the Lake, see Figure 1; and 2) a *computational model* that consists of a tightly coupled two-dimensional shallow water circulation/spectral wave energy evolution model.

2 Methodology

The current hydrodynamic model used by the Lake Erie Operational Forecast System or LEOFS is the Princeton Oceanic Model or POM. The POM model was developed primarily by Dr. Alan Blumberg and Dr. George Mellor in the late 1970's and uses a sigma coordinate (vertical), curvilinear coordinate (horizontal), free surface, ocean model that also uses a turbulent sub-model. The current POM version used by GLOFS has been modified by Dr. David Schwab of NOAA's Great Lakes Environmental Research Laboratory (GLERL) and by researchers from The Ohio State University. As its input, The model takes surface meteorological data, such as surface wind speed and air temperature, which are obtained from, for example, U.S. and Canadian meteorological buoys (nowcast mode) and the National Weather Services operational North American Mesoscale (NAM) weather forecast model (forecast mode). However, the current models inability to accurately model the nearshore region of Lake Erie has induced the idea that a new model may need to be used to capture this region of Lake Erie.

Besides POM, other potential hydrodynamic models include ADCIRC, GEMSS, QUODDY, ROMS, and DYNLET. However, the flexibility of ADCIRC to be coupled with a wave model(SWAN) makes it the easiest to use. It has been tested and validated in a variety of

different applications such as modeling tides & wind driven circulation, analysis of hurricane storm surge & flooding, dredging feasibility & material disposal studies, larval transport studies, and nearshore marine operations. The ability of ADCIRC to model wind driven circulation in the nearshore region makes it a reputable choice for usage on Lake Erie because Lake Erie is driven by wind.

2.1 Governing Equations

The three main equations that govern the ADCIRC model are the shallow water equations which are the depth-averaged continuity equation(\mathcal{L}) and the 2D momentum equation(\mathcal{M}). These hyperbolic PDEs are derived from the Navier-Stokes equations which are the general equations for fluid motion and are:

$$\mathcal{L} \equiv \frac{\partial \zeta}{\partial t} + \nabla \cdot \mathbf{q} = 0 \quad (1)$$

$$\mathcal{M} \equiv \frac{\partial \mathbf{q}}{\partial t} + \nabla \cdot (\mathbf{q}\mathbf{q}/H) + \tau_{bf}\mathbf{q} + \mathbf{f}_c \times \mathbf{q} + gH\nabla\zeta - \varepsilon\Delta\mathbf{q} - \mathbf{F} = \mathbf{0} \quad (2)$$

The equations above are able to solve the 3 unknowns ζ , u and v . From Equation 1, ζ is the height or elevation of the free surface and $\mathbf{q} \equiv (Hu, Hv)$, where the total height of the water column, $\zeta + h_b$, is H and where u and v are the depth-integrated horizontal velocities or currents. The distance from the datum to the bottom or bathymetric depth(positive downward) is h_b . The constant surface elevation or datum in the case of Lake Erie is set at 184 meters above sea level. The reference datums for bodies of water are generally taken when the water is still. From Equation 2, the bottom friction factor is τ_{bf} , the Coriolis force is \mathbf{f}_c , acceleration due to gravity is g , the eddy viscosity coefficient is ε , and \mathbf{F} can potentially, depending on the inputs, contain multiple stresses and forces such as wave radiation stresses, wind radiation stresses, variable atmospheric pressure, and tidal potential forces.

2.2 ADCIRC

The *Advanced CIRCulation model for oceanic, coastal and estuarine water* or ADCIRC was created as a means of solving 2D and 3D time dependent, free surface circulation and transport problems. ADCIRC offers the user the ability to run in serial or in parallel which allows for faster simulation run times. It also uses the continuous Galerkin method in solving the finite element mesh.

ADCIRC uses the 2D Momentum Equations as they appear in Equations 2; however, they make various manipulations of the Continuity Equation in 1 to create the Generalized Wave Continuity Equation or GWCE, and can be written as:

$$\frac{\partial \mathcal{L}}{\partial t} + \nabla \cdot \mathcal{M} + \tau_0 \mathcal{L} = 0 \quad (3)$$

The GWCE is a weak weighted residual that is solved by ADCIRC along with the 2D momentum equation. During the manipulations of these equations, a user-defined weighting

factor, τ_0 , is created. This weighting factor weights the relative contribution of the primitive wave portions of the GWCE. τ_0 is basically a factor that needs to be adjusted and fine tuned to disperse the solution enough as to not cause oscillatory solutions in your model so it runs smoothly. The τ_0 variable is something that only exists in the continuous Galerkin method, CG, version of ADCIRC and not the discontinuous Galerkin method, DG, version of ADCIRC.

Carrying out the partial time derivative of \mathcal{L} and and the $\nabla \cdot \mathcal{M}$ from Equation 3, the GWCE is expanded into:

$$\frac{\partial^2 \zeta}{\partial t^2} + \tau_0 \frac{\partial \zeta}{\partial t} + \frac{\partial J_x}{\partial x} + \frac{\partial J_y}{\partial y} - uH \frac{\partial \tau_0}{\partial x} - vH \frac{\partial \tau_0}{\partial y} = 0, \quad (4)$$

where:

$$J_x = -uH \frac{\partial u}{\partial x} - vH \frac{\partial u}{\partial y} + \mathbf{f}_c v H - \frac{g}{2} \frac{\partial \zeta^2}{\partial x} - gH \frac{\partial}{\partial x} \left(\frac{P_{H_20}}{g\rho_0} - \alpha\eta \right) + \frac{\tau_{sx,winds} + \tau_{sx,waves} - \tau_{bx}}{\rho_0} + (M_x - D_x) + u \frac{\partial \zeta}{\partial t} + \tau_0 u H - gH \frac{\partial \zeta}{\partial x}, \quad (5)$$

$$J_y = -uH \frac{\partial v}{\partial x} - vH \frac{\partial v}{\partial y} + \mathbf{f}_c u H - \frac{g}{2} \frac{\partial \zeta^2}{\partial y} - gH \frac{\partial}{\partial y} \left(\frac{P_{H_20}}{g\rho_0} - \alpha\eta \right) + \frac{\tau_{sy,winds} + \tau_{sy,waves} - \tau_{by}}{\rho_0} + (M_y - D_y) + v \frac{\partial \zeta}{\partial t} + \tau_0 v H - gH \frac{\partial \zeta}{\partial y}, \quad (6)$$

and the vertically-integrated momentum equations determine the currents by:

$$\frac{\partial u}{\partial t} + u \frac{\partial u}{\partial x} + v \frac{\partial u}{\partial y} - \mathbf{f}_c v = -g \frac{\partial}{\partial x} \left(\zeta + \frac{P_{H_20}}{g\rho_0} - \alpha\eta \right) + \frac{\tau_{sx,winds} + \tau_{sx,waves} - \tau_{bx}}{\rho_0 H} + \left(\frac{M_x - D_x}{H} \right), \quad (7)$$

and:

$$\frac{\partial v}{\partial t} + u \frac{\partial v}{\partial x} + v \frac{\partial v}{\partial y} - \mathbf{f}_c u = -g \frac{\partial}{\partial y} \left(\zeta + \frac{P_{H_20}}{g\rho_0} - \alpha\eta \right) + \frac{\tau_{sy,winds} + \tau_{sy,waves} - \tau_{by}}{\rho_0 H} + \left(\frac{M_y - D_y}{H} \right), \quad (8)$$

where the atmospheric pressure at the water surface is P_{H_20} , the reference density of water is ρ_0 , the Newtonian equilibrium tidal potential is η , and the effective earth elasticity factor is α ; the surface stresses caused by winds and waves are $\tau_{sx,winds}$, $\tau_{sy,winds}$, $\tau_{sx,waves}$, and $\tau_{sy,waves}$; the bottom stresses are τ_{bx} and τ_{by} ; the lateral stress gradients are M_x and M_y , and the momentum dispersion terms are D_x and D_y . The unknown water level (ζ) and currents (u and v) can be computed by ADCIRC using a linear Lagrange interpolation and solving these expanded Equations 4, 7, and 8 for the three degrees of freedom at every node of the finite element mesh.

2.2.1 ADCIRC Inputs

There are 5 input files that are read by ADCIRC in which 2 of them are required and the other 3 are conditional depending on what your simulation needs are. The *Grid and Boundary Information File* or fort.14 is required and is the the actual finite element mesh that you wish to use. The finite element mesh and the boundary conditions types need to be established in this file. The *Model Parameter and Periodic Boundary Condition File* or fort.15 is the other required input file. The fort.15 file contains most of the parameters required to run ADCIRC. Some of these parameters include the timestep interval, run duration, ramping function options, the τ_0 value you wish to use, meteorological wind/pressure interval, normal flow boundary flow rates, and the station's longitude & latitude for which you would like to have data written for and the interval at which the data should be written. The *Single File Meteorological Forcing Input* or fort.22 is used to inform ADCIRC the number the meteorological fields to be used, the offset that the meteorological data starts in comparison to the start time of the ADCIRC run(if there is one), and the wind velocity multiplication factor. The *Multiple File Meteorological Forcing Input* or fort.221 & fort.222 are the methods used to force the Lake Erie model other than river flows. The fort.221 contains atmospheric pressure recorded by stations around Lake Erie and are measured in units of Pascals(millibars). The fort.222 contains wind velocity in the u and v components from recording stations around Lake Erie at 10 meter heights above the water surface and are in units of m/s .

Once the pressure and wind velocities are read into ADCIRC, the following relationships are computed;

$$P_{H_{20}} = \frac{P}{100 \times g \times \gamma_{H_{20}}} \quad (9)$$

$$W_S = \|W_V\| \quad (10)$$

$$D_C = 0.001 \times (0.75 + 0.067 \times W_S) \quad (11)$$

$$W_{ST} = D_C \times 0.001293 \times W_V \times W_S \quad (12)$$

where P is the atmospheric pressure read from the fort.221, $\gamma_{H_{20}}$ is the density of water, W_S is the wind speed, W_V is the wind velocity read from the fort.222, D_C is the drag coefficient, and W_{ST} is the wind stress. If the calculated D_C is greater than 0.003, then the D_C is set to 0.003.

2.2.2 ADCIRC Outputs

ADCIRC has multiple outputs from which we can use to verify against recorded data at specified meteorological that the model is working; such as, the elevation time series or surface elevation (fort.61), the atmospheric pressure time series(fort.71), and the wind velocity time series(fort.72). The elevation time series is the most important output from ADCIRC, because unlike the atmospheric pressure and wind velocity, the change in the water surface elevation is not an input into ADCIRC. Because of this, matching the recorded surface elevation to the ADCIRC results goes a long way into verifying the model. The depth-averaged

velocity time series (fort.62) cannot be compared with recorded data because there are no recordings for depth averaged velocity in Lake Erie; however, it can be used to compare the differences in the depth-averaged velocity the ADCIRC+SWAN results.

Another way of validating the model is comparing the significant wave heights recorded at the 3 meteorological buoys that are all located in the open water. However ADCIRC only solves the modified forms of the Shallow Water Equations so it is unable to determine the significant wave heights. This is why the SWAN model, one that can model the wave heights, is coupled with ADCIRC so this validation is possible.

2.3 ADCIRC + SWAN

Simulating Waves Nearshore or SWAN was developed to determine wave propagation in time and space, shoaling, refraction due to current and depth, frequency shifting due to currents and non-stationary depth. For our model, the most important physics that SWAN accounts for is the wave generation by wind because as mentioned before, Lake Erie is primarily a wind driven lake. Other physics that SWAN accounts for are white capping, depth-induced breaking, dissipation due to vegetation, and diffraction. The SWAN equation, \mathcal{S} , accounts for the wave action density $N(\lambda, \varphi, \sigma, \theta, t)$ as it moves through geographic space (λ, φ) and spectral space (with relative frequencies σ and direction θ), in time (t) , the action balance equation is governed by:

$$\begin{aligned} \mathcal{S} \equiv \frac{\partial N}{\partial t} + \frac{\partial}{\partial \lambda} [(c_\lambda + u) N] + \arccos \varphi \frac{\partial}{\partial \varphi} [(c_\varphi + v) N \cos \varphi] \\ + \frac{\partial}{\partial \theta} [c_\theta N] + \frac{\partial}{\partial \sigma} [c_\sigma N] = \frac{S_{tot}}{\sigma} \end{aligned} \quad (13)$$

where (u, v) are the ambient current, (c_λ, c_φ) are the group velocities, c_θ is the propagation velocity in the θ -space, and c_σ is the propagation velocity in the σ -space. S_{tot} is the source term that represents how the wind determines the growth of the waves by:

- surf breaking and bottom friction,
- action lost due to whitecapping,
- and action in deep water and shallow water of the exchange between spectral components caused by nonlinear effects.

SWAN communicates with ADCIRC in order to obtain the necessary wind speeds, water levels, and currents that ADCIRC calculates at each node. These three components are essentially what drives the SWAN model. For a given timestep, these components are first calculated by ADCIRC, then they are passed onto SWAN where it recalculates the water level and all related wave processes. These SWAN values are then read back into ADCIRC at each node where the process repeats itself for the next timestep. When running ADCIRC+SWAN, only one of the models can run at once because each model needs information from the other in order to force it. The radiation stress gradients, $\tau_{sx,waves}$ & $\tau_{sy,waves}$, partially drive and force ADCIRC and are computed by SWAN by the following equations;

$$\tau_{sx,waves} = -\frac{\partial S_{xx}}{\partial x} - \frac{\partial S_{xy}}{\partial y}, \quad (14)$$

$$\tau_{sy,waves} = -\frac{\partial S_{xy}}{\partial x} - \frac{\partial S_{yy}}{\partial y}, \quad (15)$$

where the wave radiation stresses are S_{xx} , S_{xy} and S_{yy} . The radiation stresses, which are constant on each element, are interpolated into the space of continuous, piecewise linear functions and differentiated to obtain the radiation stress gradients in Equations 14 & 15. The wave radiation stresses are computed at the mesh node and are defined as;

$$S_{xx} = \rho_0 g \int \int \left(\left(n \cos^2 \theta + n - \frac{1}{2} \right) \sigma N \right) d\sigma d\theta, \quad (16)$$

$$S_{xy} = \rho_0 g \int \int (n \sin \theta \cos \theta \sigma N) d\sigma d\theta, \quad (17)$$

$$S_{yy} = \rho_0 g \int \int \left(\left(n \sin^2 \theta + n - \frac{1}{2} \right) \sigma N \right) d\sigma d\theta, \quad (18)$$

where n is the ratio of group velocity to phase velocity. Equations 16 – 18 are computed before Equations 14 & 15. An area-weighted average of the gradients is used to project the element-based gradients to the elements adjacent to each mesh node.

There are many outputs from SWAN which include average wave direction, directional spreading, wave energy, and dissipation but the most useful output is the significant wave height. This value can be compared to the recorded results from the 3 Lake Erie buoys, thus adding another comparison to help validate the model. Once validation has occurred, the wave energy can be used to determine locations for the wave energy converters.

2.4 The GLERL-Donelan Wave model

While the coupled ADCIRC + SWAN model has performed well for a number of applications, spectral wave models are known to be prohibitively expensive in terms the computational effort required; see, for example, (Mellor, 2008), which claims the SWAN model required 86 times the computer run time as the Princeton Ocean circulation model. This motivates our interest in the investigation of a simpler wave model, that has come to be known as the GLERL–Donelan wave model. Originally formulated at the Canadian Centre for Inland Waters and the US National Oceanic and Atmospheric Administrations Great Lakes Environmental Research Laboratory (GLERL), the GLERL–Donelan model is a relatively simple parametric wave model that has historically formed the basis of the US National Weather Services Great Lakes wave forecasts. In contrast to spectral and most other parametric wave models, which are based on the action balance equation, the GLERLDonelan wave model is based on the conservation of total wave momentum. This formulation avoids the need to solve the action balance equation over a (usually large) set of discrete frequency components, which is one factor that makes spectral-based models, such as SWAN, prohibitively expensive from a computational perspective.

Therefore, as part of this project we explored the development and application of a discontinuous Galerkin (DG) finite element method for a relatively simple parametric wave model, the so-called GLERL–Donelan wave model, originally developed by Mark A. Donelan

and subsequently revised by Schwab, et al, at the Great Lakes Environmental Research Laboratory (GLERL). Unlike spectral-based model, which are based on the action balance equation, the model is based on a conservation of wave momentum equation, i.e.,

$$\frac{\partial \mathbf{M}}{\partial t} + \nabla \cdot \mathbf{T} = \frac{\boldsymbol{\tau}_w}{\rho_w g}, \quad (19)$$

where $\mathbf{M} = (M_x, M_y)^\top$ is the total wave momentum vector with components in the horizontal, x and y directions, \mathbf{T} is the (symmetric) momentum flux tensor, $\boldsymbol{\tau}_w$ is the wind stress vector, g is the gravitational constant, and ρ_w is the density of water. Starting with the right-hand side of (19), the wind forcing is parameterized by

$$\frac{\boldsymbol{\tau}_w}{\rho_w} = 0.028 D_f |\mathbf{U} - 0.83 \mathbf{C}_p| (\mathbf{U} - 0.83 \mathbf{C}_p),$$

where $\mathbf{U} = (u_w, v_w)^\top$ is the wind velocity vector at 10 meters above the sea surface, \mathbf{C}_p is the wave phase velocity vector, and D_f is the form drag coefficient given by an empirical relationship.

Under the assumption of deep water linear wave theory (applicable for most wind waves on the lake surface), the momentum flux tensor has components

$$\begin{aligned} T_{xx} &= \frac{g}{2} \int_0^{2\pi} \int_0^\infty E(f, \theta) \cos^2 \theta df d\theta, \\ T_{xy} &= T_{yx} = \frac{g}{2} \int_0^{2\pi} \int_0^\infty E(f, \theta) \sin \theta \cos \theta df d\theta, \\ T_{yy} &= \frac{g}{2} \int_0^{2\pi} \int_0^\infty E(f, \theta) \sin^2 \theta df d\theta, \end{aligned} \quad (20)$$

where $E(f, \theta)$ is the wave energy spectrum, which is a function of wave frequency f and direction θ . In the GLERL–Donelan model, it is assumed that the wave energy spectrum is separable in frequency and direction, i.e., $E(f, \theta) = \tilde{E}(f)S(\theta)$, where $S(\theta)$ is assumed to have a cosine-squared angular dependence about some mean wave direction θ_0 , i.e., $S(\theta) \propto \cos^2(\theta - \theta_0)$ and $\tilde{E}(f)$ is given by the Joint North Sea Wave Project (JONSWAP) energy spectrum. Under these assumptions, the moment flux tensor components given by (20) take a relatively simple form. Preliminary numerical results obtained with a “stand-alone” DG implementation of the GLERL–Donelan model on Lake Erie are very promising in terms of both accuracy and computational efficiency (see the next section, in particular, Figure 11)

3 Principal Findings & Significance

3.1 ADCIRC+SWAN Results

The mesh on which ADCIRC+SWAN runs on was created using up-to-date shoreline that was traced and the newest bathymetry data. The resulting mesh contains 401,547 nodes connecting 782,650 elements and can be seen in Figure 1. The size of individual elements ranges from 10 meter in rivers/channels/marinas to 3 kilometers in the open water where there is little to no change in bathymetry.

Monthly simulations were run from May through October because these are the months that have the weather buoy data available to compare the model simulations to. The years that the simulations were run for were 2009, 2010, and 2011. A comparison of the weather buoys 45005, 45132, and 45142 to the ADCIRC+SWAN output for both May 2009 and August 2009 is shown in Figures 2 - 7. The gaps in the Recorded Data (blue line) indicate times in which the station was not recording. Overall the model has shown its ability to capture the peaks and general trends of the recorded data.

The maximum monthly waves heights for May 2009 and August 2009 are shown in figures 8 & 9. Computing the max height values for the entire lake at every node provides us with information on where the max elevation is most likely to occur and therefore be the best place to implement the wave energy converters.

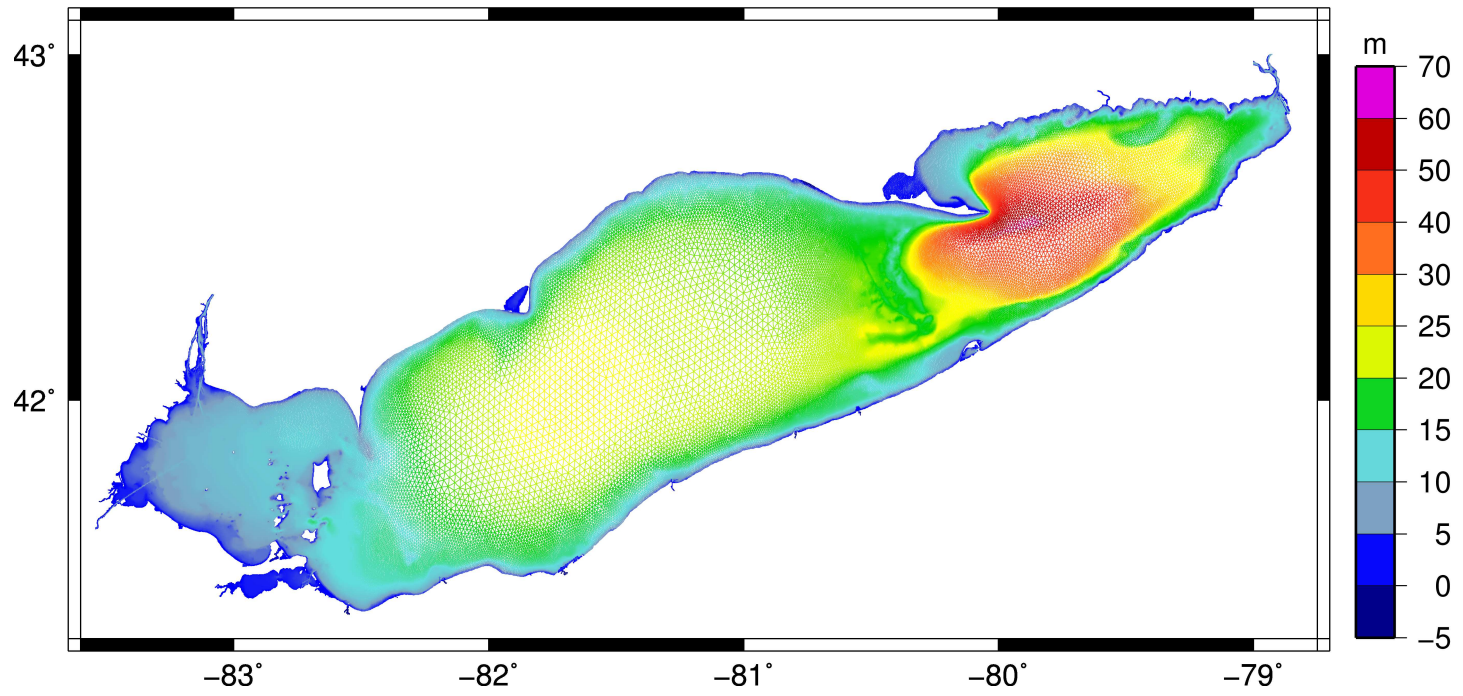


Figure 1: Lake Erie Mesh with Bathymetry

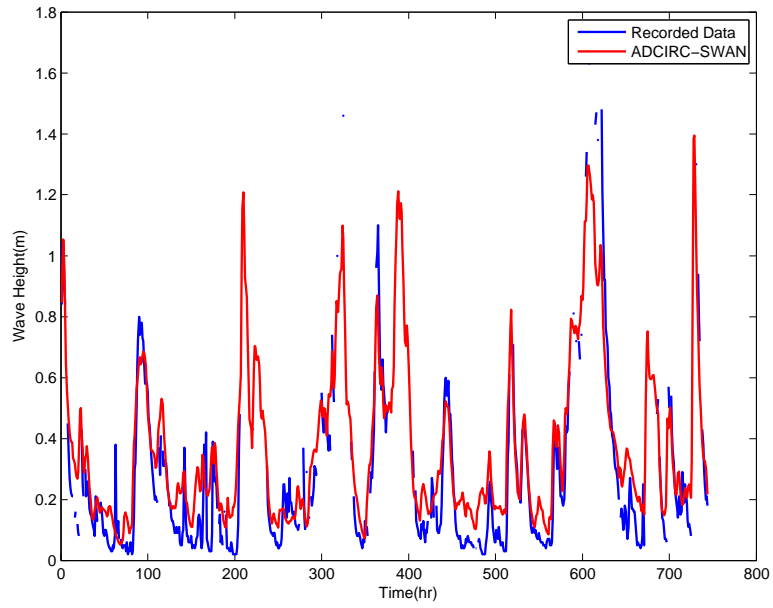


Figure 2: May 2009 Significant Wave Height at Buoy 45005

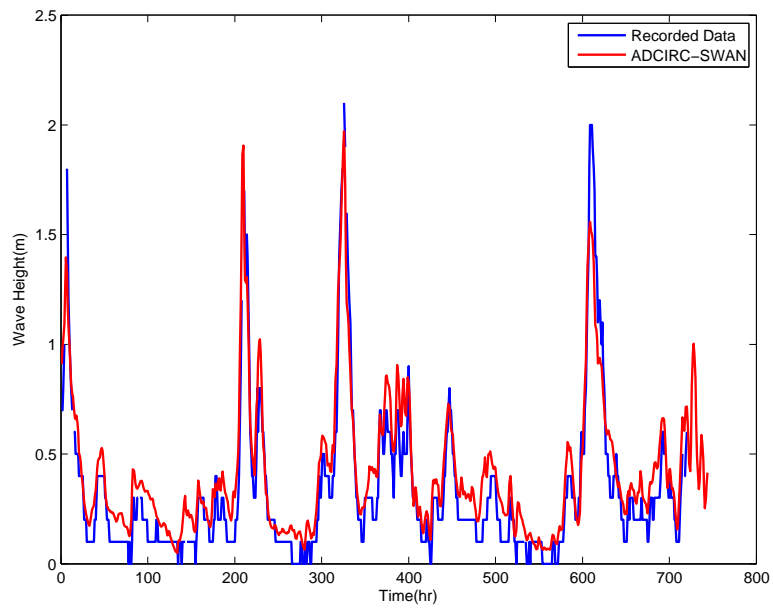


Figure 3: May 2009 Significant Wave Height at Buoy 45132

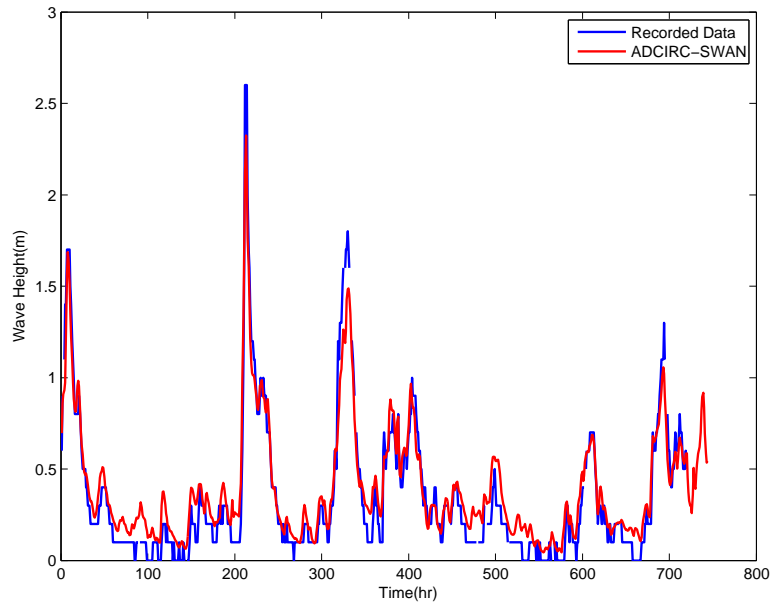


Figure 4: May 2009 Significant Wave Height at Buoy 45142

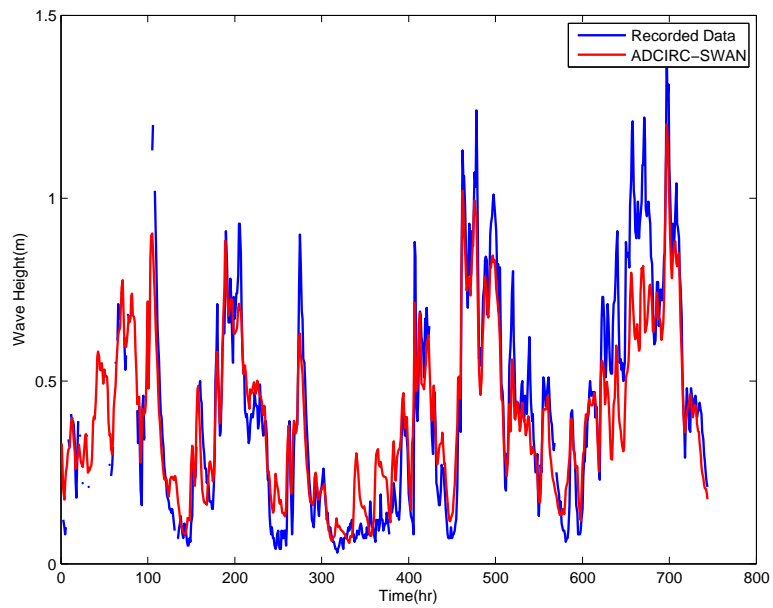


Figure 5: August 2009 Significant Wave Height at Buoy 45005

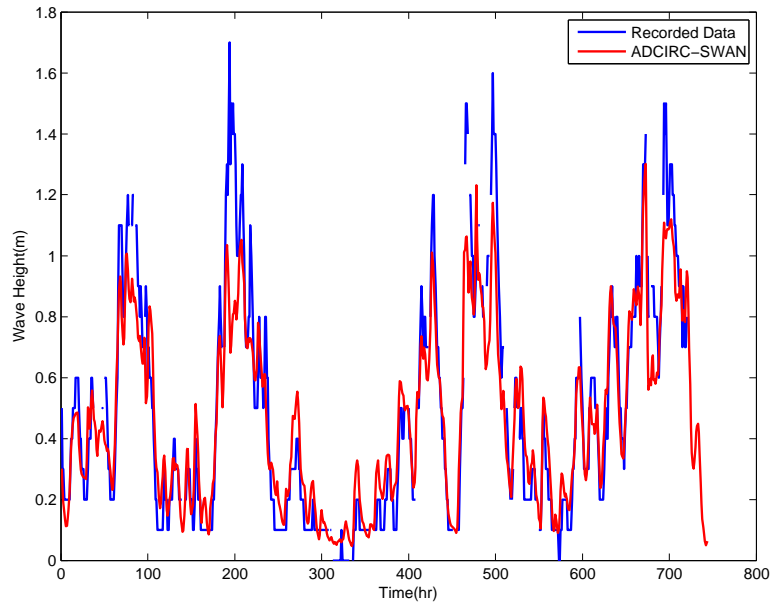


Figure 6: August 2009 Significant Wave Height at Buoy 45132

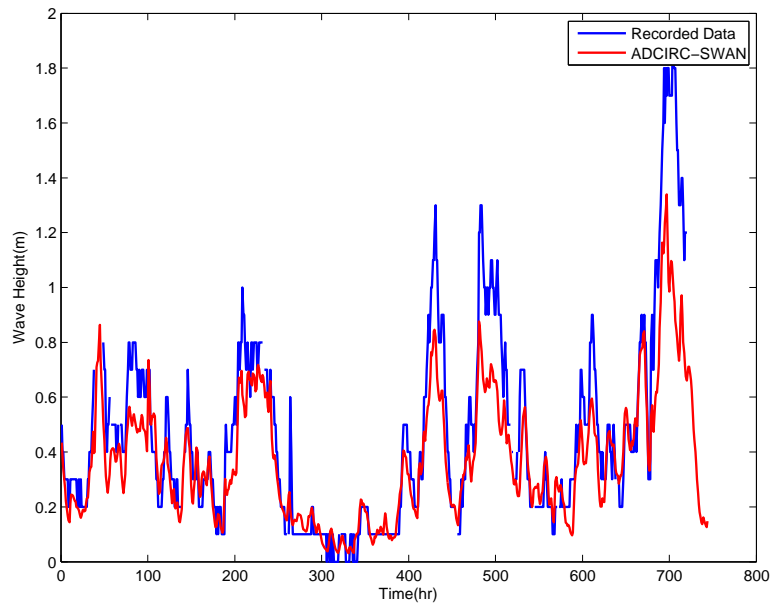


Figure 7: August 2009 Significant Wave Height at Buoy 45142

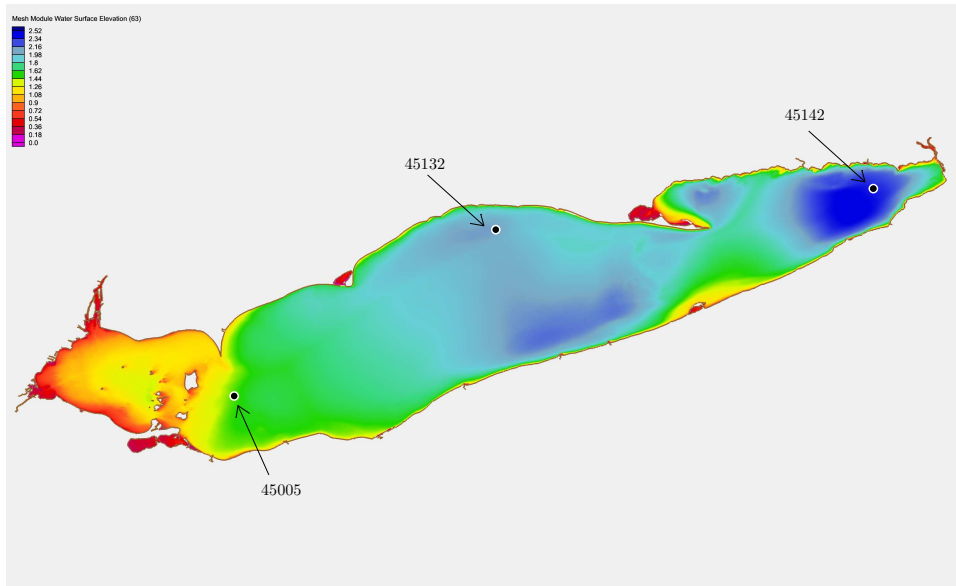


Figure 8: May 2009 Maximum Wave Heights

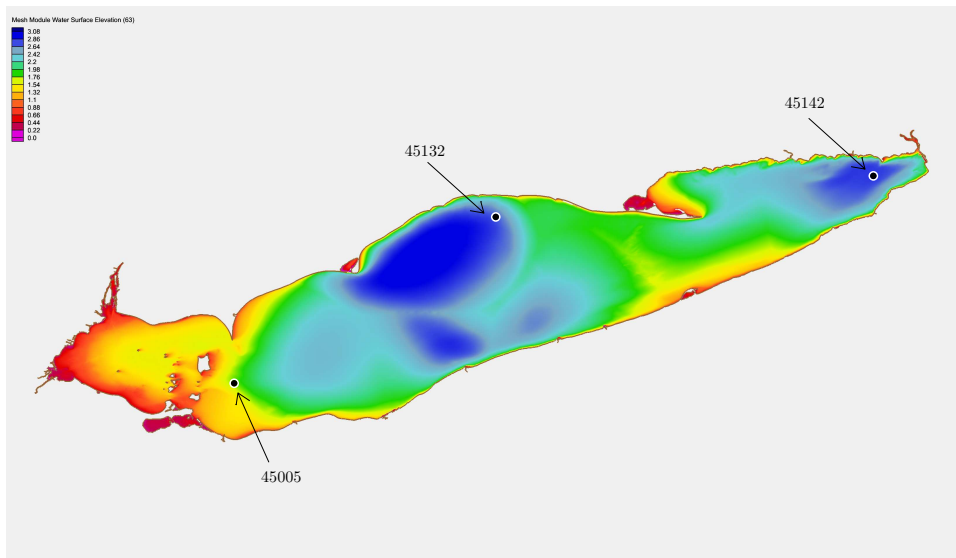


Figure 9: August 2009 Maximum Wave Heights

3.2 DG-Wave Results

Graduate student Angela Nappi is working with PI Kubatko on the development and application of the aforementioned DG method for the GLERL–Donelan wave model. Preliminary numerical results obtained with the DG GLERL–Donelan model are very promising. Verification and initial validation of the model are shown in Figures (8) and (9), respectively. The model was verified on a simple test case presented in Schwab, 1984. The domain of the test case is a 100-km diameter circular basin discretized using the mesh shown in Figure (8). A constant wind of 10 m/s is applied in the positive x direction for a duration of 24 hours. Donelan developed the following empirical relationship for characteristic wave height, H_c , as a function of fetch X , namely,

$$H_c = 0.00366g^{-0.62}X^{0.38}(U \cos \theta)^{1.24},$$

where θ is the angle between the wind and wave vectors found by maximizing the effective fetch

$$F_e = X(\cos \theta)^{2.35}.$$

A comparison of the DG solution to the empirical formula for characteristic wave height along the centerline of the circular basin ($y = 50$ km) is displayed in Figure (8). The computed correlation coefficient between the solutions is 0.944. In terms of model validation, the DG GLERL–Donelan model is applied to an unstructured mesh of Lake Erie. The mesh used for this preliminary validation test has approximately 2500 elements with a maximum element size of 5 km and a minimum size of 4 km; see Figure (8). The mesh was generated automatically using the advanced mesh generator ADMESH.

Wind forcing data is obtained from a number of recording stations around and on the Lake. Three buoys on Lake Erie record significant wave height hourly. The results for a simulation of the first full week of May 2010 are presented in Figure (9). Results from the DG GLERL–Donelan are compared to both recorded buoy data and simulation results from a SWAN simulation. In general, the model shows very good agreement with the recorded data and even out-performs SWAN in general. This is especially promising considering the relative simplicity and computational cost of the model compared to third-generation wave models.

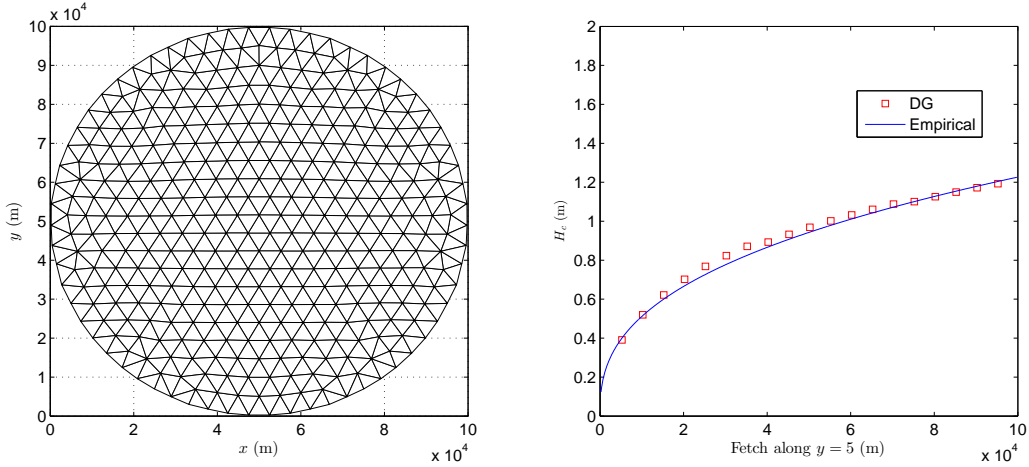


Figure 10: Plot of the finite element mesh used for the verification test case (left) and a comparison of the DG and empirical solutions along $y = 50$ km (right).

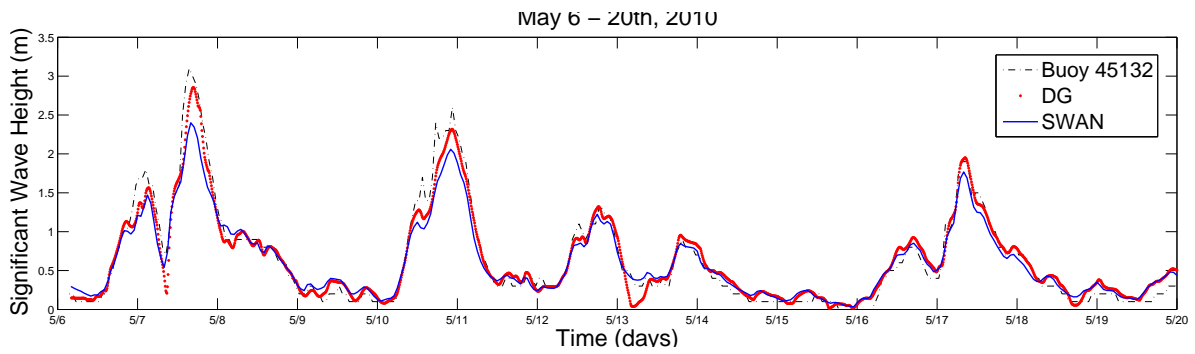


Figure 11: Numerical predictions of significant wave height in meters comparing the SWAN model (blue line) and the DG GLERL–Donelan model (red squares) to recorded buoy data.

High-performance Porous Polybenzimidazole Membranes For Water Treatment Using Forward Osmosis

Basic Information

Title:	High-performance Porous Polybenzimidazole Membranes For Water Treatment Using Forward Osmosis
Project Number:	2011OH2900
Start Date:	5/1/2011
End Date:	2/28/2013
Funding Source:	Other
Congressional District:	9
Research Category:	Engineering
Focus Category:	Treatment, Methods, Water Quality
Descriptors:	
Principal Investigators:	Isabel Escobar

Publications

1. Flanagan Michael; Isabel Escobar, submitted 2012, Novel Charged and Hydrophilized Polybenzimidazole (PBI) Membranes for Forward Osmosis, Journal of Membrane Science.
2. Flanagan Michael; Richard Hausman, Brett Digman, Isabel Escobar, Maria Coleman, TS Chung, 2011, Surface Functionalization of Polybenzimidazole Membranes to Increase Hydrophilicity and Charge. In: Escobar I.C. and B. Van der Bruggen (eds.), Modern Applications in Membrane Science and Technology. ACS Symposium Series; American Chemical Society: Washington, DC, pages 303-- 322.
3. Flanagan Michael; Richard Hausman, Isabel Escobar, Maria Coleman, TS Chung, 2012, Functionalization of Polybenzimidazole Membranes for Pore Size Reduction, Increased Hydrophilicity and Surface Charge, In 2012 AIChE Spring Meeting, Houston, TX, April 1--5.
4. Flanagan Michael; Richard Hausman, Isabel Escobar, 2011, Polybenzimidazole Forward Osmosis Membranes Functionalized to Impart Surface Charge and An Increase In Hydrophilicity, In 2011 AIChE Annual Meeting, Minneapolis, MN, October 16--21, 2011.
5. Flanagan Michael; Richard Hausman, Isabel Escobar, Maria Coleman, TS Chung, 2011, Polybenzimidazole Forward Osmosis Membranes Functionalized for Increased Surface Charge and Hydrophilicity, In 2011 NAMS Annual Meeting, Las Vegas, NV, June 4--8.
6. Flanagan M., and I.C. Escobar (2013). Novel Charged and Hydrophilized Polybenzimidazole (PBI) Membranes for Forward Osmosis, Journal of Membrane Science, 434: 85-92.
7. Flanagan M. and I.C. Escobar (2012). "Charged and Hydrophilized Polybenzimidazole (PBI) Membranes for Forward Osmosis," 2012 AIChE Annual Meeting, Pittsburgh, PA, October 28-November 2, 2012.
8. Flanagan M., and I.C. Escobar (2012) "Novel Charged and Hydrophilized Polybenzimidazole (PBI) Nanofiltration Membranes," 2012 Euromembrane Conference, London, England, September 23-27, 2012.

High-performance porous polybenzimidazole membranes for water treatment using forward osmosis

Progress Report

The University of Toledo PI: Isabel C. Escobar, Chemical and Environmental Engineering, The University of Toledo, MS 305, Toledo, OH 43606-3390, USA Tel: +1-419-530-8267, Fax: +1-419-530-8086, Email: Isabel.Escobar@utoledo.edu

Students Supported: (1) Michael F. Flanagan, MS in Chemical Engineering; and (2) Jordan Morales, undergraduate, BS in Chemical and Environmental Engineering

Publications:

1. Flanagan M., and I.C. Escobar (submitted, 2012). Novel Charged and Hydrophilized Polybenzimidazole (PBI) Membranes for Forward Osmosis, *Journal of Membrane Science*.
2. Flanagan, M., Hausman, R., Digman B., I.C. Escobar, M.R. Coleman, and T-S Chung (2011). Surface Functionalization of Polybenzimidazole Membranes to Increase Hydrophilicity and Charge. In: Escobar I.C. and B. Van der Bruggen (eds.), *Modern Applications in Membrane Science and Technology*. ACS Symposium Series; American Chemical Society: Washington, DC, pages 303-322.

Presentations:

1. Flanagan M., R. Hausman, and I.C. Escobar, M. Coleman, and T-S Chung (2012). "Functionalization of Polybenzimidazole Membranes for Pore Size Reduction, Increased Hydrophilicity and Surface Charge," 2012 AIChE Spring Meeting, Houston, TX, April 1-5, 2012.
2. Flanagan M., R. Hausman, and I.C. Escobar (2011). "Polybenzimidazole Forward Osmosis Membranes Functionalized to Impart Surface Charge and An Increase In Hydrophilicity," 2011 AIChE Annual Meeting, Minneapolis, MN, October 16-21, 2011.
3. Flanagan M., R. Hausman, I.C. Escobar, M. Coleman, and T-S Chung (2011). "Polybenzimidazole Forward Osmosis Membranes Functionalized for Increased Surface Charge and Hydrophilicity," 2011 NAMS Annual Meeting, Las Vegas, NV, June 4-8, 2011.

Problem and Research Objectives:

Forward osmosis (FO) is a technology that shows great potential as an alternative to current desalination techniques. The most attractive features of a FO membrane system include lower operational cost and less energy requirement. Unlike reverse osmosis (RO), that uses hydraulic pressure to create the driving force of water permeation, FO processes use an osmotic pressure gradient between the feed and draw solutions to create the driving force across a semi-permeable membrane. Water flows through the membrane, concentrating a saline feed solution, and diluting a draw solution of much higher osmotic pressure.

While emphasis has been placed on developing FO processes recently [1], two main drawbacks still exist. Most commercially available membranes were designed for RO processes and have proven to be less than ideal for FO systems. RO membranes are built on thick fabric support layers that suffer high levels of internal concentration polarization, significantly reducing membrane flux [2]. The second drawback involves finding an economically viable and easily separable draw solute. Many draw solutes have been examined as possible candidates for FO processes including: ammonium bicarbonate, calcium chloride, potassium bicarbonate, magnesium chloride, magnesium sulfate, and sodium bicarbonate [1, 3-4]. Ammonium bicarbonate was chosen as the draw solution solute for this study due to its ease of separation to allow for feed solute rejection studies [5-6].

To address the issue of finding a suitable membrane material for FO processes, researchers in Singapore recently developed a PBI nanofiltration (NF) hollow fiber membrane [7-8]. PBI is a polymer that exhibits high mechanical strength, thermal stability, and chemical resistance [9-10]. Through use of the phase inversion technique, asymmetric PBI membranes were formed yielding high water fluxes but low monovalent salt rejection [7-8].

PBI nanofiltration membranes from these studies showed amphoteric behavior with desirable water flux and high rejection of divalent ions. Rejection of ionic species was found to be highly dependent on the solution pH. pH values determine the phases and sizes of the ionic species, in addition to the surface charge characteristics of the PBI membrane [7-8]. It was also shown through surface modification of the PBI membranes that the rejection of aqueous solutes is highly dependent on both the membrane pore size and electrostatic interaction between the solute and membrane. Analysis of virgin and modified PBI membranes in pressure driven systems with single electrolyte solutions at various pH values showed a decrease in solute permeability with modification at neutral pH values, with increasingly higher rejection as the pH increased and the membranes took on higher surface charges [11-13].

In an attempt to enhance the properties of the PBI membranes, the authors have recently demonstrated that asymmetric flat sheet PBI membranes could successfully be cast, and functionalized, using several different modifying agents [12-13]. The previous study used 4-(chloromethyl) benzoic acid (CMBA) for an activation step and p-phenylene diamine (PD), ethylene diamine (ED), and taurine to functionalize the membrane surface. All three modifications resulted in increases in hydrophilicity and membrane surface charge. Additionally, it was hypothesized that the modifications led to decreases in the mean pore size over that of the virgin sample. Previous research with PBI membranes chemically

modified with p-xylylene has shown that modification could successfully decrease membrane pore size in the selective layer to a molecular level [11]. Modification with p-xylylene [11] involves a similar reaction to the activation step with CMBA [12-13] described previously by the authors, but has two reactive chloride groups that result in cross-linking of the PBI chains.

Recent studies have indicated that improvements in the wetting of a membrane surface can be critical in improving the membranes water permeability [14]. Lack of sufficient wetting exacerbates internal concentration polarization and disrupts continuity of water throughout the membrane structure. Decreased water continuity within the internal membrane pathways reduces the effective porosity, thus reducing water transport. This study [14] showed that by RO pretreating membranes used in FO application, or through addition of surfactants to the solutions used in the FO process, water permeability could be increased due to the enhanced wetting effect, and subsequent removal of air and vapor trapped in the porous selective layer of the membrane. Each of these techniques affected the various layers of the membrane differently depending on the structure and hydrophobicity of the layer. If the membrane surface is modified to be more hydrophilic, then the wetting effect of the membrane surface can be enhanced.

The focus of this study is to investigate the performance of the functionalized flat sheet PBI membranes in a forward osmosis application. The functionalization of membranes studied included the three modifying agents used previously, and an additional fourth modifying agent, poly(acrylamide-co-acrylic acid). Poly(acrylamide-co-acrylic acid) (PACA) was selected for this study due to its ability to crosslink with the activated PBI membrane and because of its natural properties in aqueous environments. PACA has both amino (-NH₂) and carboxyl (-COOH) functional groups that can either protonate or deprotonate based on the solution pH, and it is incredibly hydrophilic in nature [15-17]. A summary schematic of the two-step chemical modification procedure is shown in Figure 1. For simplicity, the modification of the PBI repeat unit is only shown at one of the secondary amines for one of the imidazole rings. This reaction could take place at both imidazole rings for the repeat units on the membranes surface.

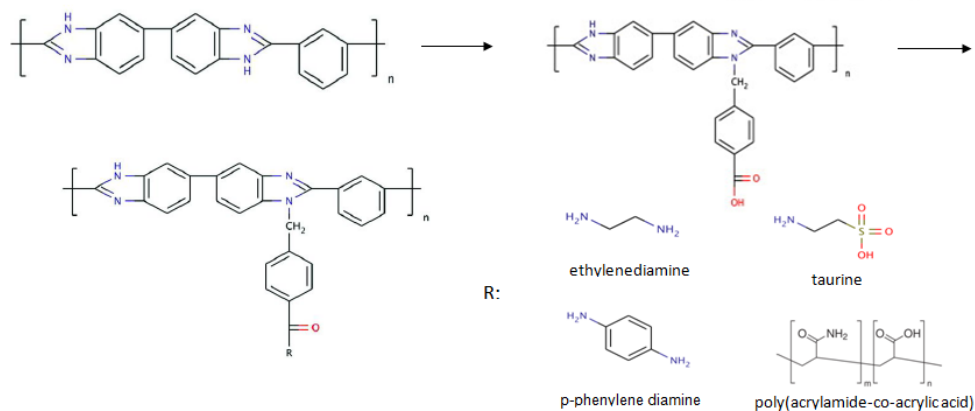


Figure 1. Chemistry for two-step modification procedure.

Methodology:

Chemicals

All chemistry required for PBI membrane casting, preparation, and surface modification used in this study has been described previously [12-13]. PBI dope was supplied by PBI Performance Products, Inc. (Charlotte, NC) as a 26 wt% solution. Ammonium bicarbonate, poly(acrylamide-co-acrylic acid), all poly(ethylene glycol) solutes, and sodium chloride were purchased from Sigma-Aldrich (USA). Glycerol, glucose, sucrose, and raffinose were purchased from Fisher Scientific (USA). DI water was supplied by a continuous distillation apparatus.

Feed and draw solutions

For all experiments the draw solution used was a 2M ammonium bicarbonate (NH_4HCO_3) solution made by dissolving reagent grade ammonium bicarbonate in DI water. The feed solutions for all experiments consisted of a 0.1M sodium chloride (NaCl) solution. The osmotic pressure gradient across the membrane was approximately 65 bar [1, 3].

Polybenzimidazole forward osmosis membranes

All PBI membranes were cast and modified in house. The casting and two-step modification procedure has been previously described [12-13]. In summary, the PBI flat sheet membranes were cast at 150 μm with a doctor's blade and formed by way of the phase inversion technique. The selective layer thickness was found to be approximately 8 μm . After formation, the surface was activated by way of reaction between the highly reactive chloride of the CMBA molecule and the secondary amine in the imidazole ring of the repeat unit in the PBI backbone. The second step involved subsequent modifications performed in a 2-(N-morpholino) ethanesulfonic acid (MES) buffer at pH 6 using N-(3-dimethylaminopropyl)-N'-ethylcarbodiimide hydrochloride (EDCH) and N-hydroxysuccinimide (NHS) chemistry. Figure 2 shows a cross-sectional view of the asymmetric virgin PBI flat sheet membrane taken by environmental scanning electron microscopy (ESEM). An FEI Quanta 3D FEG Dual Beam Electron Microscope (FEI, U.S.A.) was used to image the sample.

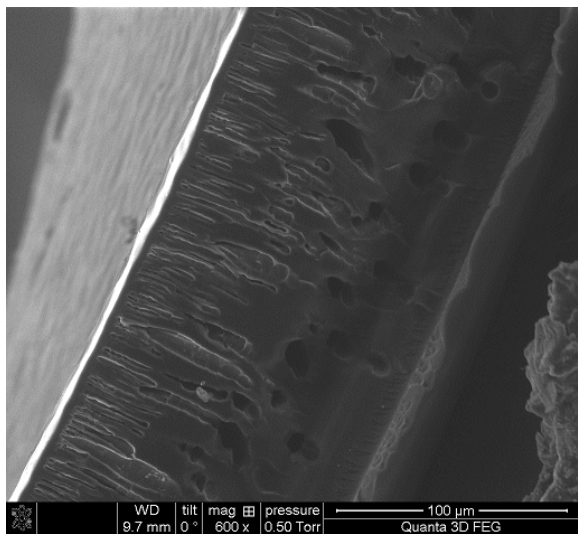


Figure 2. SEM image of the asymmetric PBI flat sheet membrane cross-section.

FTIR, contact angle, and zeta potential

The PBI membranes used in this study have previously been characterized by Fourier transform infrared spectroscopy in attenuated total reflectance mode (FTIR-ATR), contact angle, and zeta potential measurements [12-13]. FTIR analysis was obtained on a Varian Excalibur Series Fourier Transform Infrared instrument, the FTS-4000 Spectrometer and the UMA-600 Microscope (Randolph, MA). Contact angle was determined using a Tantec Model CAM-MICRO Contact Angle Meter (Tantac, Inc., U.S.A.). Surface charge was analyzed by measuring the zeta potential on the membrane surface. Samples were measured using an electrokinetic analyzer (BI-EKA, Brookhaven Instrument Corp., Holtsville, NY), located at Michigan State University. These techniques have shown the effects of PBI surface functionalization on membrane chemistry, hydrophilicity and surface charge [12-13].

Pore size determination

Total organic carbon (TOC) analysis was used to determine the pore sizes of the membranes developed. Concentrations of the solute solutions used for pore size determination were measured with a Tekmar-Dohrmann, Phoenix 8000 UV-persulfate TOC Analyzer (Tekmar Company, OH). The approach involved introducing feed solutions containing uncharged solutes (Table 1) of various Stokes-Einstein radii to the selective layer of the PBI membranes in an Amicon 8010 dead-end filtration cell (Millipore, USA). All experiments were performed as single solute permeation runs. The diluted permeate and original feed solutions were sampled in the TOC to determine solute rejection. The apparent solute rejection R (%) was calculated by Equation 1:

$$R = \left(1 - \frac{C_p}{C_f}\right) \times 100\% \tag{1}$$

where C_p and C_f are the solute concentrations in the permeate and feed solutions, respectively. The uncharged solute samples are shown in Table 1 along with their Stokes-Einstein radii [7, 15]. Nonionic

molecules have been used to determine membrane pore sizes by previous researchers [7, 11, 18-20] and a similar procedure was followed for this study.

Table 1. Molecular weights and Stokes-Einstein radii of neutral solutes for pore size determinations.

Solute	Mw (g mol ⁻¹)	Stokes radii (nm)
Glycerol	92	0.26
Glucose	180	0.37
Sucrose	342	0.47
Raffinose	504	0.58
PEG	600	0.61
PEG	1000	0.80
PEG	2000	1.41
PEG	4600	1.75
PEG	8000	2.31

200 ppm solutions were made of each individual solute in DI water. Each separation experiment involved permeation of a single solute in a pressure driven dead-end flow cell at 4.82 bar. Every membrane-solute combination was repeated three times so the average value could be calculated. The rejection values for all solutes were used to determine the mean effective pore size and the molecular weight cut-off (MWCO) for each membrane modification. The MWCO of a membrane is the molecular weight of the solute that is 90% retained by the membrane [18].

Forward osmosis operational set-up

The FO process used in this study is shown in Figure 3. The membrane filtration cell was a Sterlitech CF042 acrylic filtration cell (Sterlitech Corporation, Kent, WA) modified for forward osmosis to allow for water to flow through rectangular channels on both sides of the membrane. The channel dimensions of 8.25 cm length and 5.1 cm height provided a total membrane area of 42 cm². The 0.1M sodium chloride feed solution flowed across the selective (dense layer) side of the membrane and the 2M ammonium bicarbonate draw solution across the permeate side of the membrane. Polypropylene mesh feed spacers were used in the channels to provide membrane support and to enhance turbulence and mass transport. Variable speed peristaltic pumps (Fischer Scientific) were used to pump the liquids in co-current flow and at equal flow rates. Due to the endothermic disassociation of ammonium bicarbonate, the draw solution was allowed to equilibrate to room temperature before the FO experiments were begun. The solution was continuously mixed during the equilibration period. Both the feed and draw solutions were run at room temperature for all experiments.

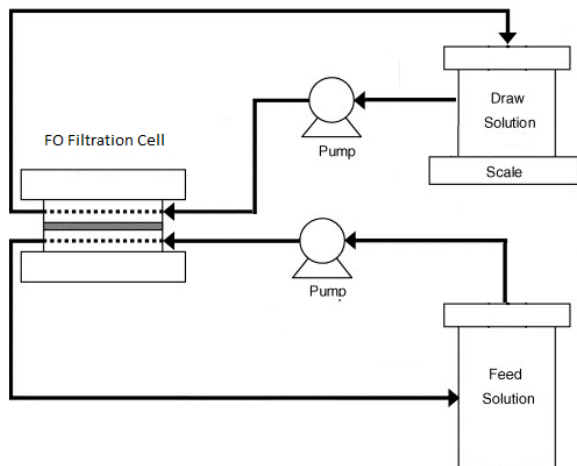


Figure 3. Schematic of co-current flow forward osmosis system.

This experimental set-up allowed for minimization of strain to the membrane as a result of unequal pressure across the length of the membrane; and to reduce the effect that additional parameters (temperature gradient, different fluid velocities, counter-current flow, etc.), other than concentration gradient, would have on the transport of feed solution across the membrane.

The initial experimental approach involved testing a 2M ammonium bicarbonate solution against feed solutions of 0.1M sodium chloride solutions, at both pH 7 and pH 10. The pH adjustments were made with concentrated sodium hydroxide solution. The flow rates of both the feed and draw solution were approximately 65 mL/min. The osmotic pressure gradient between the bulk feed and draw solutions was approximately 65 bar [1, 3].

Transport properties

Mass transport across the membrane was determined by measuring the weight change of the draw solution in one hour intervals over a five hour period. The weight of the draw solution increases as water permeates across the membrane from the feed solution by way of osmosis. The volumetric increase divided by the membrane area and the selected time period gives the water flux.

Sodium chloride transport was determined by taking a sample of draw solution, after a complete FO run, and boiling the solution until the solvent had completely evaporated. The boiling process resulted in the decomposition of ammonium bicarbonate into ammonia and carbon dioxide gases [5-6] leaving only sodium chloride and sodium hydroxide crystals remaining. The weight of the remaining crystals was measured after boiling, and the crystals were then diluted with a known volume of DI water after which the pH and conductivity were measured. The concentrations of sodium chloride solutions were measured with a conductivity meter. All solution pH values were measured with a Corning 430 glass pH-electrode and a pH meter (Corning, NY). Pure water permeability from a pressure driven process at 4.82 bar was reported previously by the authors [12-13] and were used for comparison.

In order to determine the true rejection of the chloride ion by the selective layer of the PBI membranes tested, a chloride selective electrode would be needed. However, since this was not available, a second approach involving calculating the sodium hydroxide concentration from the pH measurements of the diluted salt solutions was used. The weight of the sodium hydroxide present was determined and subtracted from the total weight of the dried salt permeate weighed before dilution. The weight of the sodium chloride sample could then be divided by the weight of the water permeate and presented as the weight fraction to be compared against the other membranes.

Principal Findings:

Membrane characterization

The FTIR-ATR spectrum for PBI and the functionalized membranes (Figure 4 and Table 2) is described in detail in Hausman et al [13] for the modifications using ED, PD, and taurine. PAcA modification is confirmed by the C=O band around 1620cm^{-1} , the band around 1645cm^{-1} associated with the N-H and NH_2 bonds, and the alkane stretch around 2900cm^{-1} . The use of this technique verified the successful modification for the CMBA surface activation and for each of the final membrane modifications.

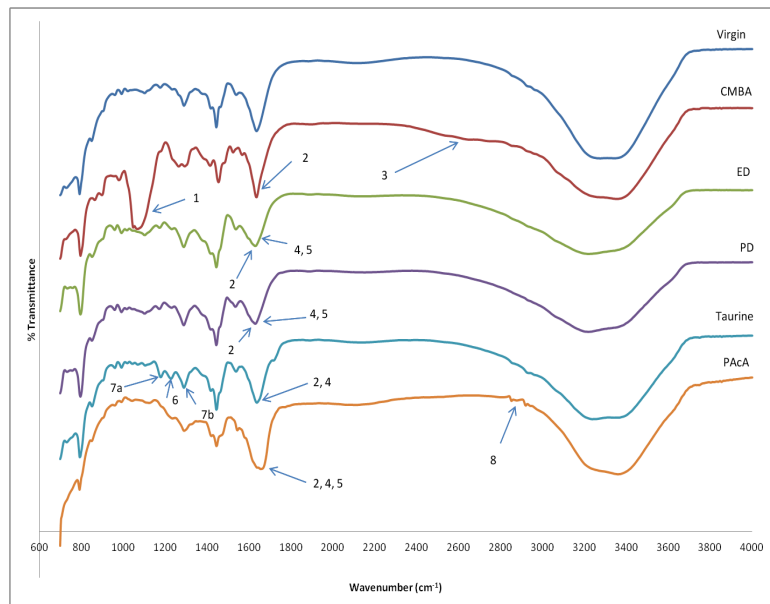


Figure 4. FTIR results for all membrane samples.

Table 2. FTIR functional group location.

Number	Functional group	Wave number (cm^{-1})
1	C–O	1057
2	C=O	1620–1640
3	OH	~ 2670
4	Secondary amine N–H	1645
5	Primary amine NH_2	1645
6	S=O	1215
7a	SO_2 (symmetrical)	1168
7b	SO_2 (anti-symmetrical)	1285
8	Alkane stretch C–H	2850–3000

Zeta potential

In previous studies [12-13] using the modification technique discussed here the final surface modifications for p-phenylene diamine, ethylene diamine, and taurine showed more charged surfaces than the virgin PBI membranes. The addition of poly(acrylamide-co-acrylic acid) for use in this study is expected to yield an even higher surface charge than the other modifications. PACA has both amino (-NH₂) and carboxyl (-COOH) functional groups that can either protonate or deprotonate based on the solution pH. In this study the pH of the feed and draw solutions for all runs equilibrated to approximately 8.3. At this pH value it is expected the carboxyl groups on the PACA membranes would be deprotonated to a significant degree (isoelectric point around 4.75) [15-16]. A membrane with a negative surface charge is expected to have a high rejection of anionic species in the feed solution.

Contact angle

Contact angle measurements for the virgin, CMBA activated, and all final modifications are shown in Figure 5. The hydrophilicity increased for all membrane modifications.

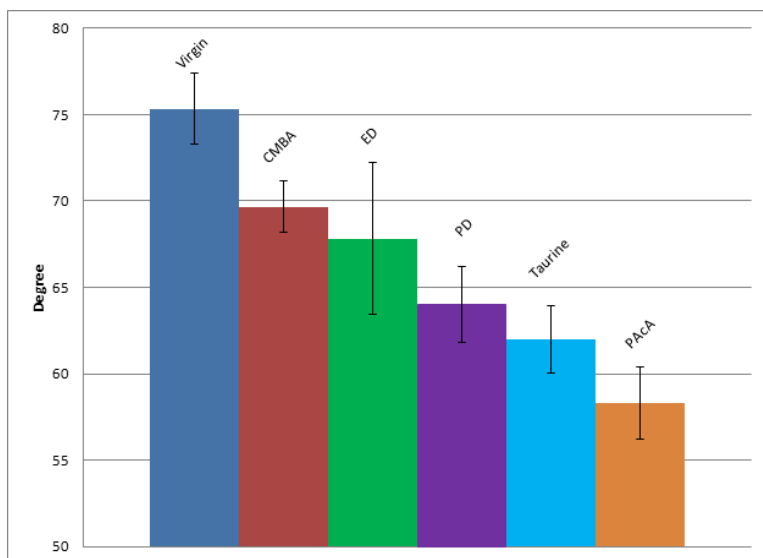


Figure 5. Contact angle measurements for all membrane samples.

Pore size determination

Table 3 shows the mean pore radius, the molecular weight cut-off, and the pore radius where the molecular weight cut off is reached. The effective mean pore sizes of all virgin and modified membranes fall in the nanofiltration range (0.5-2 nm in diameter) [7]. The effective mean pore radius of the unmodified membrane was 0.61 nm.

Table 3. Pore size data

	Virgin	CMBA	ED	PACa	Taurine	PD
Mean radii (nm)	0.61	0.45	0.38	0.41	0.37	0.33
MWCO (Da)	7977	4161	1994	1399	1287	886
MWCO radii (nm)	2.31	1.66	1.14	0.95	0.91	0.75

From Table 2 it is observed that every membrane modification showed a reduced pore size over that of the virgin. Additionally, all the final modifications showed reduced pore sizes over the CMBA activated. The ED membrane had a smaller mean pore size than the PACa but a larger MWCO. This is believed to be attributed to the large size ($M_w = 5,000,000$) and cross-linking ability of the PACa. If the large PACa molecules are bonding to multiple sites across the membrane surface in random order, the effects of steric exclusion are expected to be more pronounced on larger solutes [18-20]. As expected the taurine and PD molecules resulted in smaller pore sizes than the ED. They also showed smaller pore sizes than the PACa. The smaller pore sizes of the PD and taurine modifications over the PACa are believed to due to the smaller size of these modifying agents. The PD and taurine are small enough to permeate the pores of the activated membrane and react to a greater degree than the PACa. The large size of the PACa molecules restricts them from penetrating into the membranes pores. The effective mean pore size and MWCO for each membrane sample was calculated from a polynomial equation of the third degree. The typical rejection curves for uncharged solutes (Table 1) followed s-shaped rejection curves [18] that were analyzed with polynomial trendlines.

Forward osmosis flux results

While water permeability through all the modified membranes was lower than that of the virgin membranes in pressure-driven mode (Figure 6), water permeability through all modified membranes was greater than permeability through the virgin membranes in FO mode (Figure 7). Figure 7 shows the results of the FO flux data measured for all the membranes where the starting pH of the feed was 7. Each membrane modification was run three separate times to determine average membrane flux values. Relating this to the pure water flux data obtained for the process driven by hydraulic pressure, (pressure-driven nanofiltration process, Figure 6), it was observed that the behavior of the membranes was reversed. In the pressure-driven process [12-13], the driving force for water permeation was the hydraulic pressure (4.82 bar) applied to the membrane. In the pressure driven process, the primary resistance to water flux stemmed from the membrane morphology: mean pore size, pore size distribution, tortuosity, membrane thickness, etc. The CMBA pure water flux was found to be approximately 30% lower than the virgin membrane flux and the modified samples were all found to be 50-60% lower than the CMBA, or 65-75% lower than the virgin.

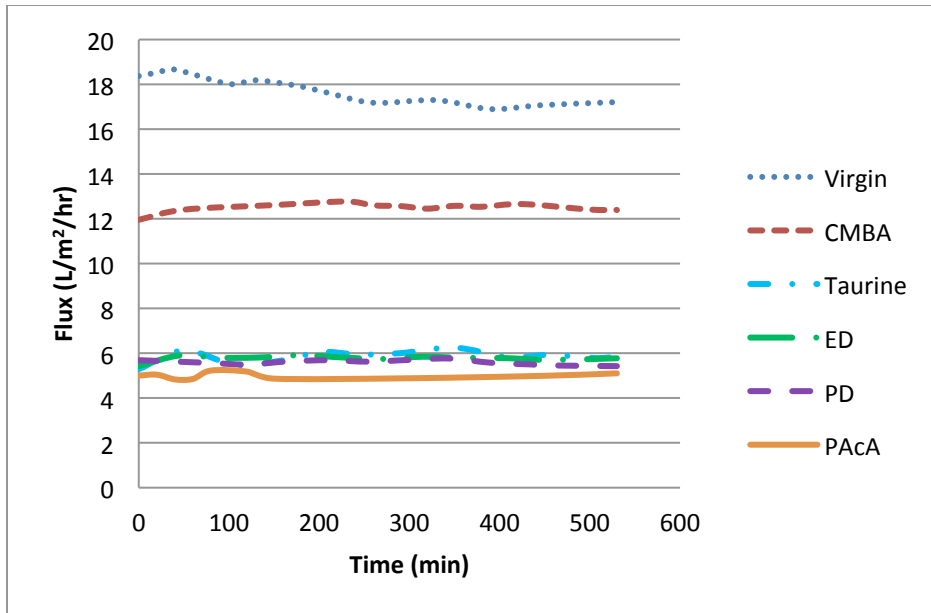


Figure 6. Flux data for all membranes in pressure driven system.

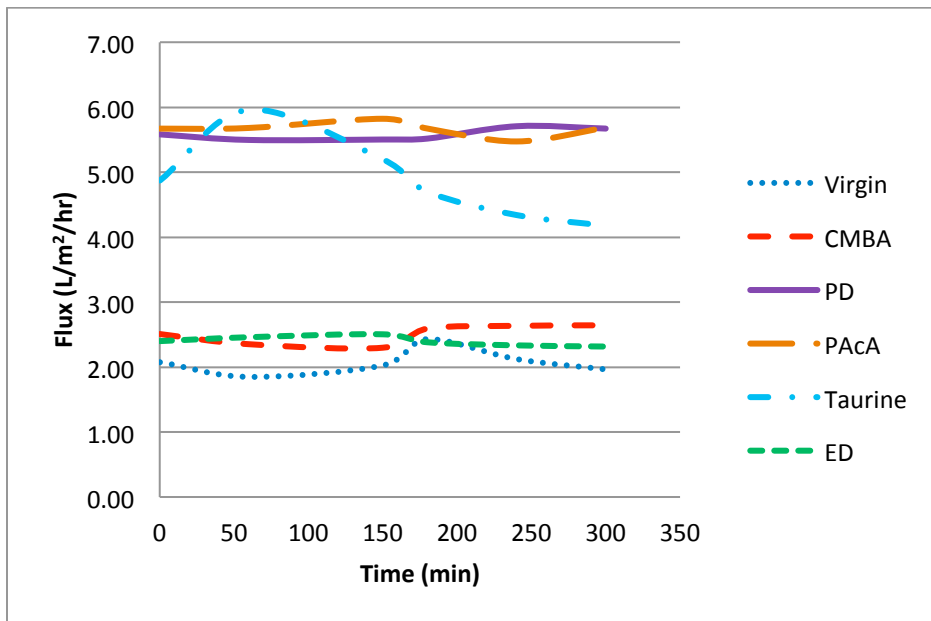


Figure 7. Flux data for all membranes in FO system

The results of the FO experiments were the reverse of those in the pressure driven experiments. The two membranes with the lowest flux in the dead-end cell were the PD and PAcA membranes. In the FO process these were the two membranes with the highest flux results. The virgin flux results were 63% and 64% lower than the PD and PAcA, respectively. The virgin was 17% lower than the CMBA and the CMBA was 55% and 56% lower than the PD and PAcA, respectively. The ED and CMBA flux values were very close to one another and not much higher than the virgin. The taurine modified membranes showed an early flux close to the PD and PAcA but began to drop lower as the run time progressed.

The performance of the membranes in FO, as opposed to the pressure driven experiments, was primarily believed to be attributed to the increased hydrophilicity of the modified membranes. In pressure driven experiments, water is forced through the membrane by hydraulic pressure, whereas in the FO system the water solution flows freely past the membrane surface. The increase in hydrophilicity of the modified membranes caused the system to favor water transport. Contact angle measurements for each of the membranes, shown in Figure 5, displayed an increased hydrophilicity after functionalization.

The contact angle for the ED membrane was the highest of the modified samples, and ED had the lowest water flux of the final modifications. Additionally, ED was the smallest of the modifying agents, but still caused a 38% decrease in the membrane pore size. The CMBA activation caused a 25% decrease. Since the hydrophilicity was slightly higher with a smaller pore size, this could explain the similar water flux between the ED and CMBA membranes. Additionally, the mean ED contact angle value was lower than the CMBA but the standard deviation was the largest and actually overlapped the lower end of the virgin standard deviation.

Despite the similar water fluxes, the weight fraction of sodium chloride in the permeate was significantly lower for the ED membranes. Previous work has shown zeta potential results for the ED modified membrane with a higher surface charge than the CMBA [12-13]. The higher surface charge and reduced pore size seems to explain the lower weight fraction of sodium chloride in the permeate while the water flux remains roughly the same as the CMBA membrane.

It is interesting to note that water transport was far lower in the FO system than the pressure-driven cell. The osmotic pressure gradient between the two bulk solutions was roughly 65 bar [1, 3], whereas the hydraulic pressure in the pressure-driven cell was only 4.82 bar. This behavior was expected and has been reported previously. Low flux results in FO systems were the result of internal concentration polarization [1-4]. Concentration polarization reduces the osmotic pressure gradient across the membrane to the point where it is significantly lower than that of the bulk. This affects the performance of the trans-membrane water transport, resulting in much lower water flux across the membrane than would be expected from the bulk osmotic pressure gradient.

Salt permeability

Due to the buffering effect of ammonium bicarbonate and sodium bicarbonate, the pH of the draw and feed solutions for the FO experiments equilibrated to a slightly basic value (approximately 8.3) where all the membranes were expected to have some degree of surface charge [12-13]. From the previous zeta potential studies involving virgin, CMBA activated, taurine, ED and PD modified at pHs 7 and 10, the readings were approximately 1.7, 4.2, -0.4, -4.5, and -7.2 mV, respectively for pH 7 and 0.1, 4.2, -3.7, -7.3, and -11.5 mV, respectively for pH 10. The rejection of 0.1M sodium chloride solutions for all modified membranes in the FO system was significantly higher than the virgin.

In a typical membrane filtration system, the percent rejection is quantified by determining the concentration of salt in the feed solution, and the concentration of the salt that permeates the membrane. Since the relationship between concentration and conductivity of sodium chloride is linear,

concentration can be determined by taking conductivity measurements of the feed initially and of the draw solution after the ammonium bicarbonate has been removed. Use of this technique would not be ideal for the process used for this discussion because the rejection values would be for a bench scale system where both the feed and draw solutions were recycled past the membrane many times over. For the 65 mL/min flow rate selected for both streams, the 1000 mL draw solution was recycled past the membrane roughly 19.5 times over a five-hour period. With 19.5 turnovers per experiment, the percent rejection values were deemed subjective. The most relevant technique for relating salt permeate data in this system is with the salt weight fractions measured for each membrane. This way, the performances of the membrane modifications can be related to one another and the virgin.

Figure 8 shows the transport ratios for the weight fraction of the sodium chloride and sodium hydroxide per water permeating the membranes, and the weight fraction of sodium chloride that permeated through the membranes. The thin bar in the back is the weight fraction of the total salt content remaining after the solvent boil off and the thicker bar in the front is the weight fraction for just the sodium chloride. From Figure 8, it is clear that every modified surface yielded higher rejection of sodium chloride over that of the virgin. The surface charges of the modified membranes were greater than the virgin at these slightly basic pH values. Additionally, the pore sizes of the modified membranes were smaller and resulted in better rejection. Due to the hygroscopic nature of sodium hydroxide and sodium chloride, the weight readings of the dried salt samples were not entirely accurate. As the heated beaker and remaining salt sample were left to cool some water moisture was trapped and added to the final weight. While the inaccuracy of the salt measurements may negate this as quantitative data, the weight measurements do provide excellent qualitative data to compare the modified samples to one another and to the unmodified.

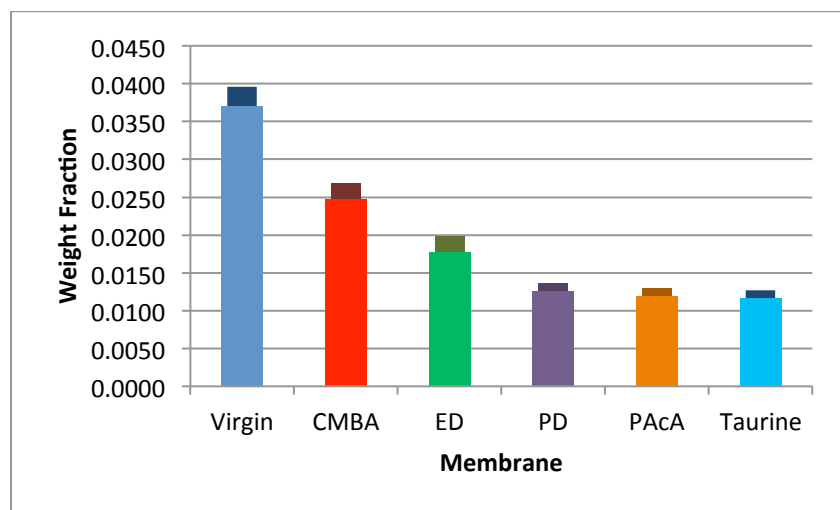


Figure 8. Total salt (back, thin bar) and sodium chloride (front, thick bar) weight fractions for each membrane.

pH effects

It was clear after only a few experimental runs that testing a feed solution at pH 10 was an impractical endeavor since the buffering strength of the much more concentrated ammonium bicarbonate draw

solution equilibrated the pH of both feed and draw solution streams. This effect was observed because both the feed and draw solutions were recycled past the membrane surface, resulting in several turnovers of the process volumes. In addition, one experiment was attempted to bring the draw solution pH up to 10, using ACS grade ammonium hydroxide, but resulted in such a large dilution that the approach was discredited. To bring the pH of 1L of draw solution to 9.98 required 400mL of ACS grade ammonium hydroxide (28-30%), diluting the solution to only 1.43M ammonium bicarbonate, and lowering the osmotic pressure gradient to approximately 47 bar. In a true desalination process, the feed solution would not be recycled past the membrane, and the pH equilibration would not be as prevalent. Even after this experiment however, when the solutions were boiled down and rehydrated to determine sodium chloride rejection, the pH of the final salt solutions of both the feed and draw followed the same trend as seen with all the other samples.

It was observed for all membrane-pH samples that after the five hour run time, the pH of both feed and draw solutions were equilibrated. Previous studies have shown high rates of reverse salt diffusion for ammonium bicarbonate draw solutions [3-4]. For the samples where there was no pH adjustment for either the feed or draw solutions, and also for the samples where the feed was adjusted to pH 10, the final pH of the feed and draw solutions was always between 8.2-8.4 (this pH range is resultant of the presence of sodium bicarbonate and sodium carbonate which buffer in this pH range). For the experiment with both feed and draw pH values initially around 10, both streams remained around 10.

At the end of a full FO run, a known volume of draw solution was boiled down until all the water evaporated. During this boiling process, all the dissolved ammonium salts decompose into ammonia and carbon dioxide. The remaining solid was then diluted with DI water to the original volume, so information about the salt rejection and membrane performance could be obtained. All the membrane experiments, including the experiment where the initial pH values were both at 10, followed the same behavior. After the boil off, and subsequent dilution, the pH of the draw solution was over 10, and the pH of the feed solutions was neutral.

These results indicate membrane selectivity of the sodium ions over the chloride ions in the feed stream. This membrane behavior was expected for the slightly basic environment where the membrane takes on a negative surface charge. In addition to surface charge, the anionic species are larger than the cationic. The larger size of the anions leads to an increased size exclusion effect from the dense membrane structure. Considering the pH equilibration for the readings taken immediately after the five-hour experimentation time, but the large pH discrepancy after the solutions were boiled down and diluted, it seems the membrane allowed passage of sodium and ammonium ions much more freely than their anion counterparts.

The selectivity of the membrane for sodium ions was balanced by the reverse diffusion of the small and positively charged ammonium ions, thus obeying the electroneutrality principle. The excess of sodium ions permeating the PBI membranes yielded the higher pH values in the diluted draw solutions. When the draw solution was boiled down the ammonium and bicarbonate ions degrade into ammonia, carbon dioxide, and water. The remaining solute crystals, after completion of boiling, were a mixture of sodium chloride and sodium hydroxide. In the feed solution however, the thermal decomposition of the ionic

species leads to a breakdown of all the ammonium and bicarbonate ions. The excess ammonium and chloride ions decomposed into ammonia and hydrogen chloride. With the continued heating, the hydrogen chloride was also boiled off as vapor, and the remaining salt was simply sodium chloride. The pH of the diluted salt solution for the feed was thus neutral.

This pH phenomenon is a qualitative confirmation of the membranes selectivity for the cationic species, and higher rejection of the anionic species. The higher rejection was attributed to both steric exclusion and Donnan exclusion. The presence of sodium hydroxide in the diluted solution gave an elevated conductivity reading, and thus shows a lower sodium chloride rejection value when conductivity readings are taken. If conductivity readings were used solely to measure salt rejection then the percent rejection values would appear far lower than the actual values.

Significance:

The overall lower mass transport across the virgin membrane in FO mode, despite the larger pore sizes, was believed to be due to the membranes higher hydrophobicity. All the modified membranes were more hydrophilic than the unmodified samples. The more hydrophilic surfaces should undergo an increased wetting effect, where the membrane-fluid interactions favored water transport. In addition to the effect of the more hydrophilic surfaces, the charged membrane surfaces showed a higher degree of sodium chloride rejection when examined as weight fractions of the permeate transporting through the membranes.

The results of PBI surface functionalization with the intent to increase hydrophilicity, increase surface charge, and decrease the membrane pore size show enhanced membrane performance both with respect to water flux and salt rejection. The reduced pore size coupled with the use of a feed stream carrying divalent or larger ions mixed with colloidal particles may have the ability to yield excellent results and high purity water. In addition, if the cations chosen were much larger (e.g. transition metals or contaminants in industrial wastewaters) then the overall salt rejection would be expected to increase.

References:

1. T.Y. Cath, A.E. Childress, M. Elimelech, Forward Osmosis: Principles, applications, and recent developments, *J. Membr. Sci.* 281 (2006) 70-87
2. J.R. McCutcheon, M. Elimelech, Influence of concentrative and dilutive internal concentration polarization on flux behavior in forward osmosis, *J. Membr. Sci.* 284 (2006) 237-347
3. N.H. Hancock, T.Y. Cath, Solute coupled diffusion in osmotically driven processes, *Environ. Sci. and Technol.*, 43 (2009) 6769-6775
4. A. Achilli, T.Y. Cath, A.E. Childress, Selection of inorganic-based draw solutions for forward osmosis applications, *J. Membr. Sci.* 364 (2010) 233-241
5. J.R. McCutcheon, R.L. McGinnis, M. Elimelech, A novel ammonia-carbon dioxide forward (direct) osmosis desalination process, *Desalination* 174 (2005) 1-11
6. J.R. McCutcheon, R.L. McGinnis, M. Elimelech, Desalination by ammonia-carbon dioxide forward osmosis: Influence of draw and feed solution concentrations on process performance, *J. Membr. Sci.* 278 (2006) 114-123
7. K.Y. Wang, T.S. Chung, J.J. Qin, Polybenzimidazole (PBI) nanofiltration hollow fiber membranes applied in forward osmosis process, *J. Membr. Sci.* 300 (2007) 6-12
8. J.L. Lv, K.Y. Wang, T.S. Chung, Investigation of amphoteric polybenzimidazole (PBI) nanofiltration hollow fiber membrane for both cation and anions removal, *J. Membr. Sci.* 310 (2008) 557-566
9. L.C. Sawyer, R.S. Jones, Observations on the structure of first generation polybenzimidazole reverse osmosis membranes, *J. Membr. Sci.* 20 (1984) 147

10. K.D. Kreuer, A. Fuchs, M. Ise, M. Spaeth, J. Maier, Imidazole and parazole-based proton conducting polymers and liquids, *Electrochim. Acta.* 43 (1998) 1281
11. K.Y. Wang, Y. Xiao, T.S. Chung, Chemically modified polybenzimidazole nanofiltration membrane for the separation of electrolytes and cephalexin, *Chem. Eng. Sci.* 61 (2006) 5807-5817
12. M. Flanagan, R. Hausman, B. Digman, I.C. Escobar, M. Coleman, T.S. Chung, Surface Functionalization of Polybenzimidazole Membranes to Increase Hydrophilicity and Charge, *Mod. Appl. in Membr. Sci. and Technol.* 18 (2011) 303-321
13. R. Hausman, B. Digman, I.C. Escobar, M. Coleman, T.S. Chung, Functionalization of polybenzimidazole membranes to impart negative charge and hydrophilicity, *J. Membr. Sci.* 363 (2010) 195-203
14. J.R. McCutcheon, M. Elimelech, Influence of membrane support layer hydrophobicity on water flux in osmotically driven membrane processes, *J. Membr. Sci.* 318 (2008) 458-466
15. E. Turan, T. Caykara, Swelling and network parameters of pH-sensitive poly(acrylamide-co-acrylic acid) hydrogels, *J. of Appl. Polym. Sci.* 106 (2007) 2000-2007
16. A. Thakur, R.K. Wanchoo, P. Singh, Structural parameters and swelling behavior of pH sensitive poly(acrylamide-co-acrylic acid) hydrogels, *Chem. Biochem. Eng. Q.* 2 (2011) 181-194
17. A. Jha, S. Agrawa, A. Mishra, J.P. Rai, Synthesis, characterization and flocculation efficiency of poly(acrylamide-co-acrylic acid) in tannery waste-water, *Iran. Polym. J.* 10 (2001) 85-90
18. C.M. Tam, A.Y. Tremblay, Membrane pore characterization – comparison between single and multicomponent solute probe techniques, *J. Membr. Sci.* 57 (1991) 271-287
19. S. Singh, K.C. Khulbe, T. Matsuura, P. Ramamurthy, Membrane characterization by solute transport and atomic force microscopy, *J. Membr. Sci.* 142 (1998) 117-127
20. S. Lee, G. Park, G. Amy, S.K. Hong, S.H. Moon, D.H. Lee, J. Cho, Determination of membrane pore size distribution using the fractional rejection of nonionic and charged macromolecules, *J. Membr. Sci.* 57 (1991) 271-287

Microbial Modulation of Acidic Coal Mine Drainage Chemistry: Implications for Passive Treatment of Minewater

Basic Information

Title:	Microbial Modulation of Acidic Coal Mine Drainage Chemistry: Implications for Passive Treatment of Minewater
Project Number:	2012OH250B
Start Date:	3/1/2012
End Date:	8/31/2013
Funding Source:	104B
Congressional District:	OH-013
Research Category:	Biological Sciences
Focus Category:	None, None, None
Descriptors:	
Principal Investigators:	John M. Senko

Publications

1. Brantner, J.S., Hotchkiss, S.T., Senko, J.M. 2013. Adaptation of soil-associated microbial communities to intrusion of acidic coal mine drainage: implications for Fe(II) removal. Environmental Science & Technology. In preparation.
2. Brantner, J.S., Milsted, A., Senko, J.M. Microbial modulation of acidic coal mine drainage chemistry: implications for passive treatment of minewater. American Society for Microbiology General Meeting Abstracts. Denver, CO. May 2013.
3. Senko, J.M. Microbially mediated iron cycling in acid mine drainage. Department of Biological Sciences Seminar. Missouri University of Science & Technology. Rolla, MO. November, 2013.
4. Senko, J.M. Microbially mediated iron cycling in acid mine drainage. Department of Geological Sciences Seminar. Ohio University. Athens, OH. May, 2012
5. Senko, J.M. Adaptation of soil-associated microbial communities to intrusion of acid mine drainage. Invited talk. Society for Industrial Microbiology Annual Meeting. San Diego, CA. August 2012.

Microbial Modulation of Acidic Coal Mine Drainage Chemistry: Implications for Passive Treatment of Minewater

John Senko (PI)

Department of Geoscience

The University of Akron

senko@uakron.edu

PRINCIPAL FINDINGS AND SIGNIFICANCE

Background and Research Objectives

We have identified several acid mine drainage (AMD)-impacted systems in which the acidic, dissolved Fe(II)-rich fluids emerge at the terrestrial surface from underground coal mine works. At these systems, AMD flows over the surface in a “sheet-flow” fashion with a water depth of approximately 0.5 cm. The AMD sheet flow characteristic of these systems facilitates the aeration of the initially anoxic AMD, and enhances the activities of aerobic Fe(II) oxidizing bacteria (FeOB). FeOB catalyze the oxidation of Fe(II) to Fe(III) at greater rates than could be achieved via the abiotic reaction between Fe(II) and O₂ at the pH associated with these systems (pH = 3.0 – 4.5). The biogenic Fe(III) subsequently hydrolyzes and precipitates as a variety of Fe(III) (hydr)oxide phases, giving rise to extensive Fe(III) (hydr)oxides that are referred to as iron mounds. In some cases, the oxidative precipitation of Fe from AMD leads to removal of ≥90% of dissolved Fe from AMD. Since removal of Fe from AMD is one of the most pressing treatment objectives of AMD treatment, the activities associated with these iron mounds could be exploited to achieve this goal. These sheet flow systems are quite remarkable, since none of these sites have received human intervention to stimulate Fe removal. As such, iron mounds could serve as inexpensive and sustainable approaches to AMD treatment. Implicit in the development of these iron mounds is the fact that at some point in time, “pristine” soil (i.e. unimpacted by AMD) was infiltrated by AMD, inducing shifts in the microbial communities associated with the systems that culminated in the microbial communities that are currently capable of robust Fe(II) oxidizing activity.

However, the dynamics of this adaptation is unclear. In this 2012 OWRC-USGS-funded project, we sought to answer the following questions:

- 1) Is the robust Fe(II) oxidizing activity associated with iron mounds attributable mostly to a) microorganisms that are suspended in AMD and “delivered” to the formerly pristine soil, b) microorganisms associated with pristine soil, or c) synergistic interaction between microorganisms associated with both AMD and pristine soil?
- 2) Do microbial communities associated with AMD and pristine soil develop robust Fe(II) oxidizing activities that are comparable to those of mature iron mound sediments?
- 3) What changes in microbial community composition accompany the development of robust Fe(II) oxidizing bacterial activities?

With an eye toward the development of “designed” iron mounds for AMD treatment, it has been suggested that “seeding” sediments with material (and associated microorganisms) from mature iron mounds could enhance the development of robust Fe(II) oxidizing microbial activities, so we asked the additional question:

- 4) Does the addition of iron mound sediment (and associated microorganisms) to pristine soil facilitate the more rapid development of robust Fe(II) oxidizing activities?

Methodology

AMD, iron mound sediments, and pristine soil (nearby soil that was unimpacted by AMD) were collected from an AMD-impacted system in North Lima, OH that is referred to as the Mushroom Farm (Figure 1). All experiments were conducted as semi-continuous reactor experiments, in which 5 g of iron mound sediment and/or soil were suspended in 50 ml of AMD and incubated under oxic conditions. For experiments to evaluate the relative contributions of AMD- and soil-associated microorganisms to the development of Fe(II) oxidizing activities, incubations were conducted using non-sterile AMD and non-sterile soil, filter-sterilized AMD and non-sterile soil, non-sterile AMD and heat-deactivated soil, and filter-sterilized AMD and heat-deactivated soil, as a negative control. To roughly approximate the continuous infiltration of AMD into sediments/soil, 25 ml of fluid was periodically removed from reactors and replaced with fresh AMD. Dissolved Fe(II) and pH were periodically measured throughout the experiments. Experiments to determine whether rates of Fe(II) oxidation increased with continuous incubation of AMD with pristine soil were conducted as described above, and included reactors that contained 5 g of iron mound sediment, 5 g of pristine soil, or 4 g pristine soil with 1 g of iron mound sediment suspended in 50 ml of AMD. In addition to dissolved Fe(II) and pH, FeOB abundances (as colony forming units per unit volume in reactor; CFU/ml) were determined in periodically removed samples using a solid medium that specifically targets aerobic microorganisms capable of using Fe(II) as an electron donor. First-order rate constants for Fe(II) oxidation (k) were calculated by linear least squares regression fitting of $\ln[\text{Fe(II)}]$ vs. time (t) using the equation:

$$\ln[\text{Fe(II)}_t] = -kt + \ln[\text{Fe(II)}_{\text{initial}}]$$

Samples were also periodically removed from the reactors, and genomic DNA was extracted for evaluation of microbial communities associated with the sediments/soil using nucleic acid-based approach targeting partial sequences of 16S rRNA genes of microorganisms associated with the soils/sediments.

Principal Findings

AMD- and soil-associated microbial contributions to Fe(II) oxidation. Initial rates of Fe(II) oxidation were highest in incubations containing non-sterile soil and non-sterile AMD, and oxidative precipitation of Fe was incomplete in incubations containing filter-sterilized AMD and heat-deactivated soil after 28 d of incubation (Figure 2 and Table 1). While initial rates of Fe(II) oxidation in incubations containing either non-sterile soil and filter-sterilized AMD or heat-deactivated soil and non-sterile soil than those that contained non-sterile soil and AMD (Figure 2), the rates of Fe(II) oxidation in all incubations except the sterile controls reached comparable levels in all incubations after three exchanges with fresh AMD (Table 1). Based on these results, it appears that the development of robust Fe(II) oxidizing bacterial activity is due to synergistic activities of microorganisms associated with soil and AMD.

Development of Fe(II) oxidizing activities. The rates of biological Fe(II) oxidation far exceeded abiotic oxidation of Fe(II) in all incubations (Figure 3). Fe(II) oxidation was incomplete in incubations containing pristine soil and pristine soil amended with iron mound sediment, and did

not occur in incubations containing iron mound sediment only (Figure 3), suggesting that the majority of oxidative precipitation of Fe(II) was attributable to microbiological activity. In incubations containing pristine soil or pristine soil with iron mound sediment, pH decreased as Fe(II) oxidation proceeded, due to hydrolysis and precipitation of biogenic Fe(III) (Figures 3 and 4). Incubations were reamended with fresh AMD 11 times, and with successive replacements of AMD, the rates of Fe(II) oxidation increased (Table 2), suggesting that the microbial communities associated with the soils/sediments adapted to continuous intrusion of AMD. The amendment of soil with iron mound material appeared to decrease the number of exchanges required to achieve maximal rates of Fe(II) oxidation (Table 2), suggesting that the use of material from existing iron mounds could be a useful approach to enhance the development of robust Fe(II) oxidizing activity in “engineered” iron mounds.

Characterization of microbial communities associated with soil/sediment incubations. After 24 d of incubation, abundances of FeOB were highest in incubations containing iron mound sediment and soil amended with iron mound sediment (1×10^4 and 6×10^3 , respectively). While FeOB could not initially be detected in incubations containing pristine soil only, their abundance increased to approximately 1×10^3 after 24 d of incubation. After 0, 6, 12, 18, and 24 d of incubation, DNA was extracted from incubations after washing of soils and sediments with ammonium oxalate, to remove Fe(III) (hydr)oxides. Additionally, DNA was extracted from organisms associated with pristine soil, iron mound sediment, and AMD. High quality genomic DNA was recovered from all samples. DNA recovered from each sample was shipped to Molecular Research LP (Shallowater, TX) for 454 pyrosequencing. As of May 13, 2013, all samples have been shipped to Molecular Research LP, but data has not been returned to the investigators.

Significance

The results that we report here are quite striking in that they illustrate the rapid rate at which microbial communities associated with pristine soil adapt to intrusion of AMD, resulting in rapid rates of Fe(II) oxidation. The robust Fe(II) oxidizing activities appear to be attributable to some type of synergistic activities of microorganisms associated with the formerly pristine soil and microorganisms suspended in the AMD that may colonize the soil. We observed that this adaptation is quite rapid, with combined soil- and AMD-associated microorganisms catalyzing Fe(II) oxidation at rates comparable to iron mound sediment after one exchange with fresh AMD. This response appears to be enhanced by the addition of iron mound material (with associated microorganisms). It is anticipated that evaluation of the shifts in microbial communities associated with the incubations will provide insight into the dynamics of the microbial community adaptation, and perhaps identify the organisms that are principally responsible for Fe(II) oxidation. Additionally, the microbial community analysis that we are carrying out will include approximately 10,000 partial sequences of 16S rRNA genes, provide the most comprehensive view of the microbial communities associated with iron mounds to date.

PUBLICATION CITATIONS

Brantner, J.S., Hotchkiss, S.T., Senko, J.M. 2013. Adaptation of soil-associated microbial communities to intrusion of acidic coal mine drainage: implications for Fe(II) removal. *Environmental Science & Technology*. In preparation.

Brantner, J.S., Milsted, A., Senko, J.M. Microbial modulation of acidic coal mine drainage chemistry: implications for passive treatment of minewater. American Society for Microbiology General Meeting Abstracts. Denver, CO. May 2013.

Senko, J.M. Microbially mediated iron cycling in acid mine drainage. Department of Biological Sciences Seminar. Missouri University of Science & Technology. Rolla, MO. November, 2013.

Senko, J.M. Microbially mediated iron cycling in acid mine drainage. Department of Geological Sciences Seminar. Ohio University. Athens, OH. May, 2012.

Senko, J.M. Adaptation of soil-associated microbial communities to intrusion of acid mine drainage. Invited talk. Society for Industrial Microbiology Annual Meeting. San Diego, CA. August 2012.

NUMBER OF STUDENTS SUPPORTED

This grant supported the work of two students at The University of Akron. It is anticipated that both students will be included as co-authors of the manuscript that is in preparation for *Environmental Science & Technology*.

Justin Brantner (PhD, Integrated Biosciences; in progress; justin3@zips.uakron.edu) received salary (Summer 2012) and material support through this project.

Shane Hotchkiss (BS, Biology; May 2013; sth8@zips.uakron.edu) received material support through this project. Shane is pursuing opportunities as a high school teacher.

AWARDS OR ACHIEVEMENTS

No awards of achievements have resulted from this work, thus far.



Figure 1. Various field site photographs of the Mushroom Farm. A) Google Earth image of the Mushroom Farm. B) Iron hydroxide crust and ‘sheet flow’ conditions of the Mushroom farm. C) Abandoned residence front yard view of iron hydroxide ‘sheet flow.’ D) Close-up image of the iron hydroxide mound formed under ‘sheet flow’ conditions.

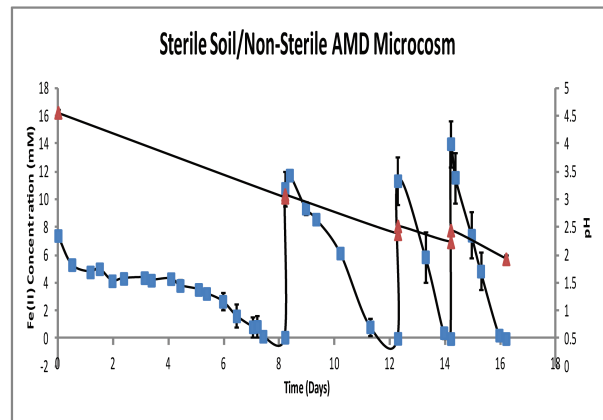
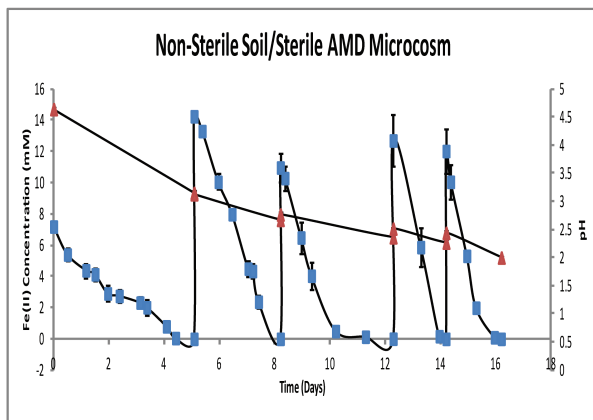
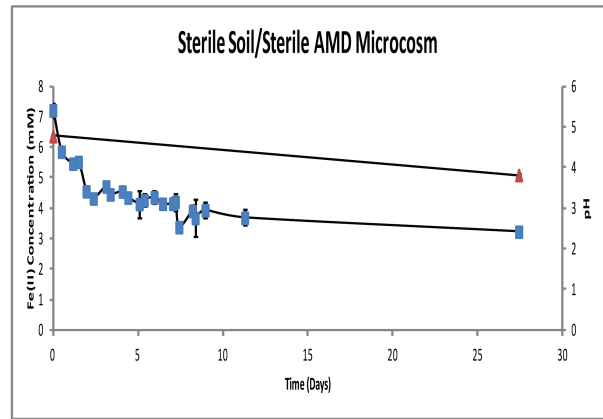
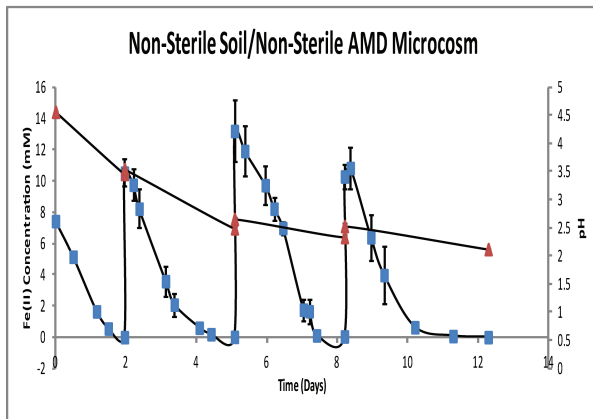


Figure 2. Dissolved Fe(II) (blue squares) and pH (red triangles) in four different microcosm incubations including pristine soil and AMD from the Mushroom Farm. Error bars = one standard deviation.

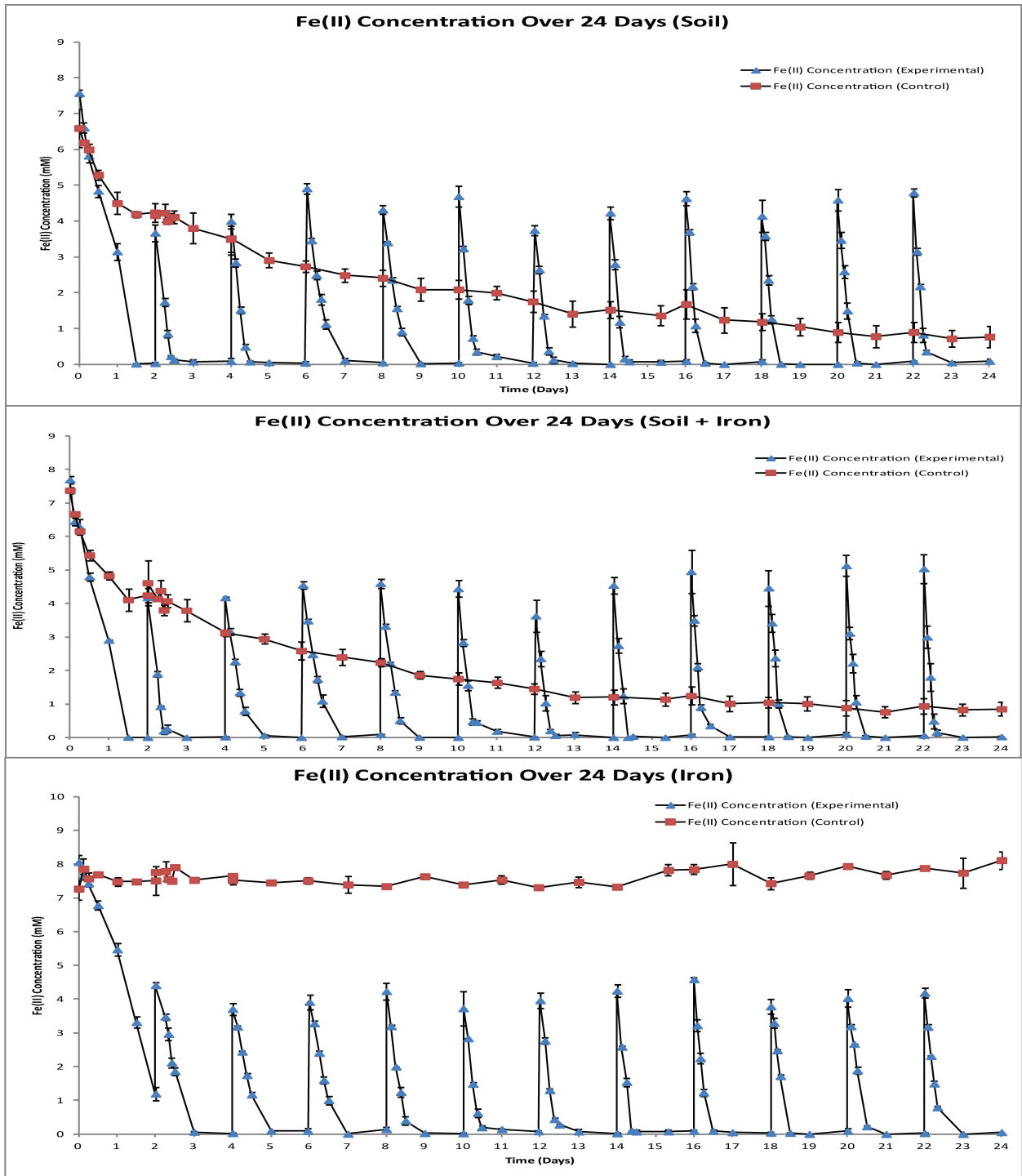


Figure 3. Dissolved Fe(II) concentrations in three different microcosm incubations over 24 days. Microcosms included: pristine soil (top panel), pristine soil amended with iron mound sediment (middle panel), and iron mound sediment (bottom panel). Blue triangles represent Fe(II) concentrations in non-sterile incubations. Red squares represent Fe(II) concentrations in formaldehyde-deactivated controls. Error bars = one standard deviation of triplicate incubations.

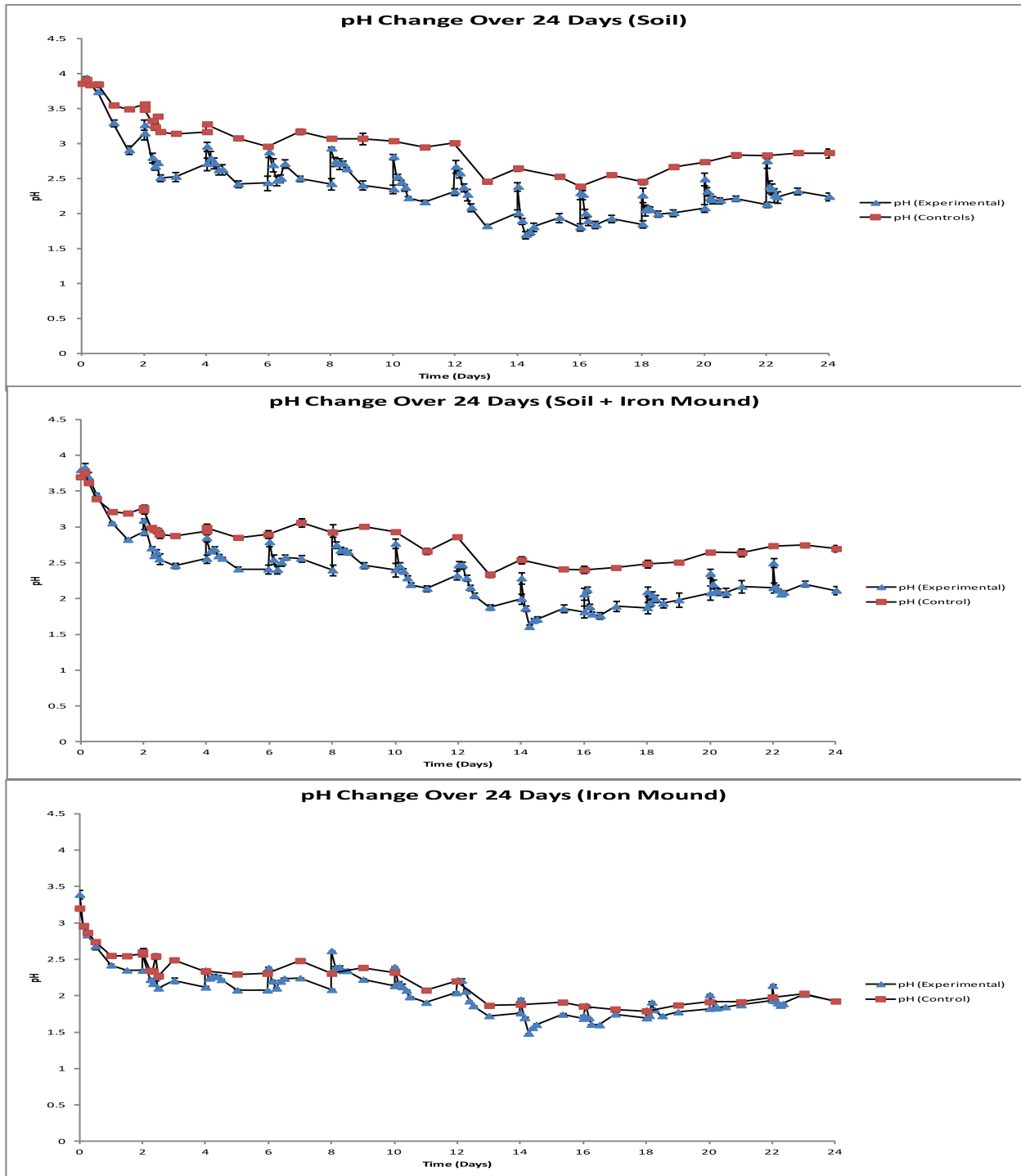


Figure 4. pH of three different microcosm incubations over 24 days. Microcosms included: pristine soil (top panel), pristine soil amended with iron mound sediment (middle panel), and iron mound sediment (bottom panel). Blue triangles represent pH of non-sterile incubations. Red squares represent pH of formaldehyde-deactivated controls. Error bars = one standard deviation of triplicate incubations.

Identification of Microcystin Degrading Bacteria in the Grand Lake St. Marys and Lake Erie Western Basin

Basic Information

Title:	Identification of Microcystin Degrading Bacteria in the Grand Lake St. Marys and Lake Erie Western Basin
Project Number:	2012OH254B
Start Date:	3/1/2012
End Date:	2/28/2013
Funding Source:	104B
Congressional District:	OH-017
Research Category:	Biological Sciences
Focus Category:	Toxic Substances, Water Quality, Treatment
Descriptors:	
Principal Investigators:	Xiaozhen Mou

Publications

1. Mou X, Jacob J, Robbins S, Lu X, Sun S and Ortiz J. 2013. Diversity and distribution of free-living and particle associated bacterioplankton community in Sandusky Bay and Adjacent Waters of Lake Erie Western Basin. Journal of Great Lakes Research. Doi: 10.1016/j.jglr.2013.02.014.
2. Ormiston A and X Mou. Temporal and spatial variability of microbial community compositions along a transect from the western basin to the central basin of Lake Erie. International Association for Great Lakes Research Annual Conference 2013. Jun 2013, West Lafayette, IN
3. Ormiston A and Mou X. Culture-based identification of microcystin-degrading bacteria in the Sandusky Bay and Maumee Bay of Lake Erie. American Geophysical Union 2013 Fall Meeting. Dec. 2012. San Francisco, CA.

Project Title: Identification of Microcystin Degrading Bacteria in Lake Erie Western Basin and the Grand Lake St. Marys

PI: Xiaozhen (Jen) Mou, Assistant Professor, Department of Biological Sciences, Kent State University, Kent OH 44242

Project ID: GRT00023315

The Western Basin of Lake Erie (LEWB) and the Grant Lake St Marys (GLSM) represent two highly eutrophic water systems in Ohio. Despite much Federal and State research and restoration efforts that have been made to regulate and monitor the nutrient loading, periodic nuisance cyanobacterial (blue-green algae, such as *Microcystis*) harmful blooms (cyanoHABs) occur every summer in recent years in these two lakes and with increased affected area, frequency and intensity. One important harmful effect of *Microcystis* blooms is the production and release of microcystin, a hepatotoxin that can be accumulated in invertebrates and cause liver damage of vertebrates, including finfish and human. Heterotrophic bacteria have been suggested as the major agents to degrade microcystin in natural environments. However, the composition and activity of the functional assemblages as well as their regulation factors are not well studied.

HYPOTHESES AND OBJECTIVES

Our proposal aims to study the microbial degradation of microcystin and taxa that carry out this function in the Grand Lake St. Marys and Lake Erie Western Basin.

Hypothesis 1. Cyanotoxin, such as microcystin, can be rapidly degraded by a diverse group of heterotrophic bacteria in lakes that are experiencing frequent harmful cyanobacterial blooms (cyanoHABs).

Objective 1: To estimate and compare microcystin degradation potentials between photo-oxidation and microbial processes in GLSM and LEWB surface water.

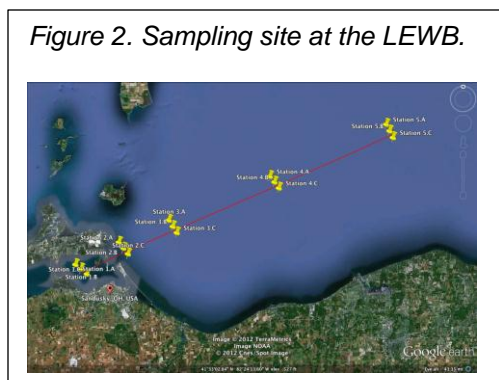
Hypothesis 2. Composition and dynamics of microcystin-degrading bacteria in LEWB and GLSM are different.

Objective 2: To determine the seasonal community structure of microcystin-degrading bacteria in the surface water of LEWB and GLSM using molecular approaches.

Objective 3: To identify environmental factors affecting the distribution and activity of microcystin-degrading bacteria.

METHODOLOGY

Sampling collection and processing. Water samples were taken from the Grand Lake St. Mary's (Figure 1) and the Sandusky Bay of Lake Erie (Figure 2) in June and July 2012. Surface



(0.5 m below air-water interface) and bottom water (0.5 m above bottom) were collected (1L) at each sample site. Immediately after sampling, sequential filtration was performed on site to pass whole water samples through 3.0 μm -pore-size and 0.2 μm -pore-size membrane filters. Original water (3 ml) and filtrates (3 ml) that passed through the 3.0 μm -pore-size filter, were preserved using 1% PFA for bacterial cell counting. Filtrates (3 L) that passed both 3 μm -pore-size and 0.2 μm -pore-size membrane filters were immediately cooled on ice and stored at 4 °C before measurements for a number of nutrients. All membrane filters were immediately cooled on ice before stored at -80 °C in the lab for molecular analysis. *In situ* parameters of water temperature, dissolved oxygen concentration (DO), conductivity and pH. Chlorophyll- α concentration were measured using an YSI hydrolab. The photic zone depth was estimated by using a Secchi disk. All samples were taken in triplicates.

Figure 1. Sampling sites and photos taken during GLSM sampling in June 2012. The dark green color of the water indicates an intense *Microcystis* bloom.



Microcosm setup and incubation

Lake water was filtered through 3.0 μm -pore-size membrane filters immediately after sampling, in order to obtain free-living bacterioplankton proportion, and to exclude bacterivores and other large particles. Filtrate was then amended with a mixture of inorganic nitrogen and phosphorus compounds and incubated in the dark at room temperature with occasional agitation for 7 days. This pre-incubation was done to allow the bacterioplankton community to consume labile dissolved organic carbon compounds and to become growth limited by carbon availability.

At the end of the pre-incubation period, microcosms were set up in 20 L acid washed carboys. Two microcosms, designated as MC-1 and MC-2, were constructed of pre-incubated lake water and amended with MC-LR ($\sim 15 \mu\text{g L}^{-1}$, final concentration). Two microcosms, designated as CT-1 and CT-2, served as controls and were constructed of pre-incubated lake water without further amendments. Microcosms were incubated in the dark at room temperature with occasional agitation for a total of 48 hours. At the end of incubation, water was filtered through 0.2 μm pore-size membrane to collect bacterial cells.

DNA extraction and pyrotag sequencing.

DNA was extracted from frozen filters using the PowerMax Soil DNA Isolation Kits (MO BIO Laboratories Inc, Carlsbad, CA) following the manufacturer's instruction. The V6 hyper-variable region of 16S rRNA genes was PCR amplified from extracted DNAs with Illustra PuRe Taq Ready-to-go PCR beads (GE Healthcare, Piscataway, NJ) using primers that were designed specifically for 454 high throughput pyrosequencing. For each sample, triplicate PCR amplifications were performed and the resulting amplicons were pooled and subsequently

examined by gel electrophoresis. PCR amplicons were purified and quantified. Equal quantity of the PCR amplicons from each sample were combined and sequenced using a Roche GS FLX sequencer. Obtained sequences will be annotated using a pipeline established by Mou Lab.

Nutrient analysis.

Concentrations of organic and inorganic nutrients, including dissolved organic carbon (DOC), total dissolved nitrogen (TND), nitrate and nitrite ($\text{NO}_3^- + \text{NO}_2^-$), ammonium (NH_4^+) and soluble reactive phosphorus (SRP) were measured using standard methods for chemical analysis for water and wastewater (APHA, 1999).

Bacterial culturing.

Bacteria in water samples collected from Sandusky Bay and Maumee Bay of Lake Erie and Grand Lake St. Mary's were isolated using the plating method. The obtained isolates were screened for their ability in degrading microcystin using MT2MicroPlates™ (Manage et al. 2009). Each well of the MT2MicroPlates™ is carbon limited, pretreated with nutrients and tetrazolium violet dye. Four concentrations (0 µg/mL, 0.1 µg/mL, 1.0 µg/mL, 10.0 µg/mL) of microcystin-LR or microcystin-RR were added to each well depending on the isolate, which acts as the carbon source for the bacteria. Color change of the well indicated that the carbon source (Microcystin-LR or Microcystin-RR) added was being used by the bacteria.

PROJECT PROGRESS AND PRINCIPLE FINDINGS

Most of the lab work has been finished, including the sampling, incubation experiment, obtaining bacterial pure culture, microcystin-degrading bacteria screening, DNA extraction, PCR, bacterial cell counting. We are currently working on performing sequencing analysis of obtained 16S rRNA gene amplicons (expected to finish by early June 2013). Nutrient analyses were delayed due to a foreseen problem with the instrument. The nutrient analysis was expected to finish by July 2013.

Based on incubation experiment, we found that both GLSM and SBLE bacteria have high potential in degrading microcystin. We have also obtained >200 pure culture of bacteria. Of the 50 isolates screened based on the BIOLOG assay, one isolate from Lake Erie was found to degrade Microcystin-LR (Isolate MCLR M26 A; Figure 3). Figure 3 also shows false positives for microcystin degradation, because the negative control wells turned purple even though no carbon source was added (such as MCLR M21 B10). To troubleshoot this issue, re-isolation of bacteria is currently happening. Figure 4 and 5 show average growth curve for MCLR M26 A and MCLR M21 B10 in the BIOLOG wells, respectively. Isolate MCLR M26 A has been confirmed with its ability of MC-degradation and will be sent out for sequencing for taxonomic identification.

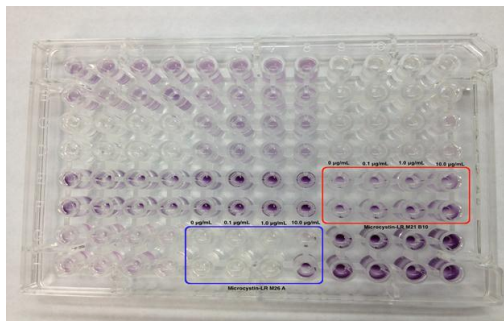


Figure 3: MT2MicroPlate™ results. The red box denotes the microcystin-LR M21 B10 isolate that showed negative results for microcystin degradation. The blue box denotes the microcystin-LR M26 A isolate that showed positive results for microcystin-LR degradation. Each well is carbon limited and is pre-treated with nutrients and tetrazolium violet. Four concentrations (0 µg/mL, 0.1 µg/mL, 1.0 µg/mL, 10.0µg/mL) of microcystin-LR or microcystin-RR were added to each well depending on the isolate, which acts as the carbon source for the bacteria. Color change indicates the usage of microcystin.

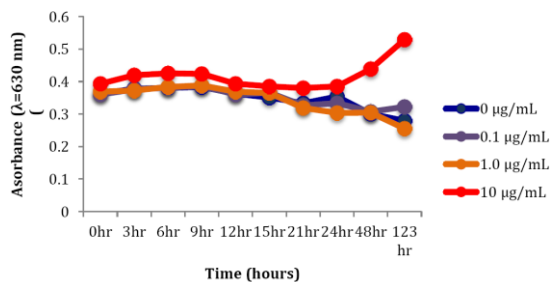


Figure 4: Average growth curve for isolate MCLR M26 A. The concentration 10.0µg/mL shows positive growth. All other concentrations followed the pattern, decreasing over time.

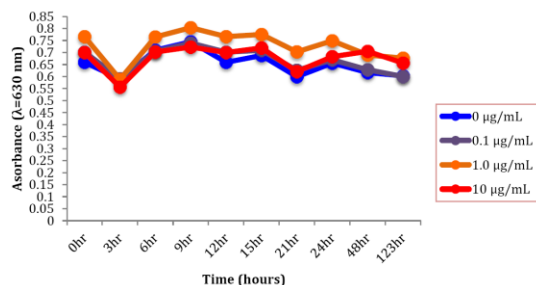


Figure 5: Average growth curve for isolate MCLR M21 B10. This is an example of an isolate screened that had negative results. The concentration 0µg/mL shows a false positive showing color change despite no carbon source was added to that well. All other concentrations followed a similar pattern, decreasing over time.

Publication citations

Mou X, Jacob J, Robbins S, Lu X, Sun S and Ortiz J. 2013. Diversity and distribution of free-living and particle associated bacterioplankton community in Sandusky Bay and Adjacent Waters of Lake Erie Western Basin. *Journal of Great Lakes Research*. Doi: 10.1016/j.jglr.2013.02.014.

Ormiston A and **X Mou**. Temporal and spatial variability of microbial community compositions along a transect from the western basin to the central basin of Lake Erie. International Association for Great Lakes Research Annual Conference 2013. Jun 2013, West Lafayette, IN.

Ormiston A and **Mou X**. Culture-based identification of microcystin-degrading bacteria in the Sandusky Bay and Maumee Bay of Lake Erie. American Geophysical Union 2013 Fall Meeting. Dec. 2012. San Francisco, CA.

STUDENTS SUPPORTED

Anna Ormiston (PhD student)

Sumeda Madhuri (PhD student)

Lawrence J Anderle (Undergraduate student)

Green-House-Gas budget of constructed wetlands: Understanding the sources to maximize benefits

Basic Information

Title:	Green-House-Gas budget of constructed wetlands: Understanding the sources to maximize benefits
Project Number:	2012OH259B
Start Date:	4/1/2012
End Date:	2/29/2014
Funding Source:	104B
Congressional District:	OH-12
Research Category:	Climate and Hydrologic Processes
Focus Category:	Wetlands, Ecology, Nitrate Contamination
Descriptors:	
Principal Investigators:	Gil Bohrer

Publications

1. Bohrer G, Zhu K, Jones RL, Curtis PS. (2013) Optimizing wind power generation while minimizing wildlife impacts in an urban area. Plos One 8:e56036.
2. Barr AG, Richardson AD, Hollinger DY, Papale D, Arain MA, Black TA, Bohrer G, Dragoni D, Fischer ML, Gu L, Law BE, Margolis HA, McCaughey JH, Munger JW, Oechel W, Schaeffer K. (2013) Use of change-point detection for friction-velocity threshold evaluation in eddy-covariance studies. Agricultural & Forest Meteorology 171:31-45.
3. Bohrer, G, Naor-Azieli, L, Mesi, S, Mouser, PJ, Stefanik, K, Schafer, KVR, and Mitsch, W 5/2012, Determining the meteorological forcing that affect seasonal and diurnal dynamics of methane emissions at a constructed urban wetland in Ohio. Oral Presentation, 30th AMS Conference on Agricultural and Forest Meteorology, Boston, MA.
4. Bohrer G, Naor-Azrieli L, Mesi S, Schäfer KVR, Mouser P, Stefanik K, Mitsch WJ, Morin T. 10/2012. Eddy flux measurements of methane at the Oletangy River Wetland Research Park wetland - Determining the seasonal and diurnal dynamics of methane emissions. Oral presentation, 4th International EcoSummit on Ecological Sustainability, Columbus, OH.
5. Schäfer KVR, Bohrer G. 10/2012. Effect of restoration on the carbon balance in the Meadowlands of New Jersey. 4th International EcoSummit on Ecological Sustainability, Columbus, OH.
6. Schäfer KVR, Bohrer G, Reid M, Tripathee R, Jaffe P. 10/2012. Temporal and spatial dynamics of methane fluxes in a temperate urban wetland. Oral presentation, 4th International EcoSummit on Ecological Sustainability, Columbus, OH.
7. Schäfer KVR, Bohrer G, Tripathee R. 4/2012. Carbon sequestration by Phragmites australis. Northeast Natural History Conference 2012, Syracuse, NY.
8. Bohrer G, Morin T, Naor-Azrieli L, Mouser PJ, Mitsch WJ, Schafer KVR. 12/2012. Determining the meteorological forcing that affect seasonal and diurnal dynamics of respiration and GPP in a constructed urban wetland in Ohio. Oral Presentation. American Geophysical Union Meeting 2012, San Francisco, CA.
9. Schafer KVR, Tripathee R, Bohrer G. 12/2012. Effect of restoration on carbon fluxes in urban temperate wetlands. Poster, American Geophysical Union Meeting 2012, San Francisco, CA.

Green-House-Gas budget of constructed wetlands: Understanding the sources to maximize benefits

10. Morin T, Bohrer G, Naor-Azrieli L, Mesi S, Schafer KVR, Stefanik K, Mitsch WJ. 11/2012. Effects of environmental conditions on an urban wetland's methane fluxes. Poster, 41st Annual Water Management Association of Ohio Conference, Columbus, OH.
11. Mesi S, Bohrer G, Naor-Azrieli L, Brooker M, Mouser P. 6/2012. Spatial-temporal intermittency of methane flux in an urban temperate wetland. Poster, 12th Annual American Ecological Engineering Society Meeting, Syracuse, NY.
12. Scannell GS, Bohrer G, Jones RL. 9/2012. Green solutions for wet weather management. Poster, 4th International EcoSummit on Ecological Sustainability, Columbus, OH.

Progress Report 2011-2012

Contract Information

Title	Green-House-Gas budget of constructed wetlands: Understanding the sources to maximize benefits
Project Number	G11AP20099
Start Date	3/1/2012
End Date	2/28/2014 (including a 12 Month no-cost extension)
Focus Category	Nitrate Contamination, Wetlands, Ecology
Keywords	Bacteria, Biotechnology, Nitrate Removal, Methane Flux, Constructed Wetlands
Lead Institute	The Ohio State University
Principal Investigators	Gil Bohrer

Abstract

Fixed nitrogen (N) is required for the growth for all biological organisms, and agriculture is dependent upon nitrogen for fertilizer. Ohio exports significant levels of nitrogen in its surface waters to Lake Erie and the Mississippi Basin due to its geology and agricultural land management techniques. Constructed wetlands can be used for nitrogen removal through the biologically-mediated process of denitrification, where nitrite is reduced to nitrogen gas and released to the atmosphere. Unfortunately, denitrification in wetlands comes with the tradeoff of increased Green House Gas (GHG) production. Wetlands sequester large amounts of carbon (C) from the atmosphere, removing the most common GHG – CO₂ but produce another and more potent GHG – methane (CH₄). In order to allow development of wetlands as a solution for N removal without concerns of GHG emissions, it is critical to understand how methane production in the wetland responds to different environmental conditions such as water and soil temperature, water chemistry. GHG emission rates and water and meteorological conditions can be measured simultaneously over wetlands using eddy-flux sensors that measure the combined emissions from a broad flux footprint area, and chamber measurements at specific points and provide spatially anecdotal and temporally sparse information. Highly variable rates of methane production and carbon sequestration at different sub-ecosystems within the wetland at a very small scale (meters) prohibits the generalization of measured environmental relationships from either eddy-flux or chamber measurements. The proposed work will use a combination of meteorological, water, and GHG flux and chamber measurements in a constructed wetland at the Olentangy River Wetland Research Center (ORWRP) over 2 years to parameterize a novel high-resolution flux footprint model. The model will be used to determine the atmospheric exchange rates of methane sources and carbon sinks at different sub-ecosystem components of the wetland. This will allow determining the strength of different environmental variables that control methane production, and will facilitate the parameterization of an empirical model to predict whole-wetland GHG budgets at ORWRP, and ultimately GHG budgets in other constructed and urban wetland ecosystems.

Methodology

We use continuous long-term eddy-covariance flux measurements to observe the rates of methane flux and the corresponding meteorological, water and soil conditions. We use a probabilistic footprint model to determine which of the tower-top observation has originated primarily from the wetland area and not from the surrounding grass, river or forest. We use an advanced neural-network model to gap-fill the flux data when an observation is missing or was filtered out. We look for empirical relationships between the meteorological, ecological and water variables in the wetland and the rates of methane flux emissions and use these observations to explain the drivers of methane flux.

Major Activity

During 2012-2013 we have update the eddy flux tower to improve methane flux measurements. In 4/2012 the old tower, 9 meter tall, was replaced by a new 17 m tall tower to account for tree growth around the tower that was making the old tower effectively too low. We also replaced the direct/diffuse PAR sensor and the methane gas analyzer, both of which were recalled by the manufacturers. We have completed the software for data analysis and processed 2 years' worth of flux and meteorological data from the wetland site. This includes the processing of the raw data, development of a new approach for despiking and data quality control, an improved footprint model, and application of an improved method for u^* filtering (developed recently with our participation, Barr et al 2013). We also completed the software and calibration of the post-processing of the data and specifically the gap-filling using an automated neural network (ANN) approach which was customized specifically for our site. We have registered the site with Ameriflux – a national open and free database of carbon and methane flux measurements and a component of a global FLUXNET database. We became the second site nationwide to report methane flux data to Ameriflux.

Preliminary Findings

Overall, our tower observations are overlapping with the wetland area. On average 55% of the signal at the tower top originated from the wetland. We sample equally all parts of the wetland and our overall footprint is rather circular and symmetric (Fig. 1). We found that the thermal state of the wetland controls a portion of the flux. Large negative (upward) longwave radiation happens when the water is warm relative to the environment. Strong incoming shortwave radiation provide heat to the water surface and strong sensible (temperature) and latent (water vapor) heat fluxes are associated with thermal gradients between the wetland and the air (Fig. 2).

Additional drivers of methane are soil temperature and ecosystem carbon exchange. We hypothesize that soil temperature controls the bacterial activity rates that produce methane. Net ecosystem exchange of carbon may be affecting methane emissions in two mechanisms – by high carbohydrate production the plants are providing more organic compounds to the soil root zone and these act as substrate to methane production, and by allowing methane to be transported through the plants aerenchyma tissue and emitted through the stomata plants provide a way for methane to avoid diffusion through the aerobic soil and water zones where it could be consumed by methane oxidizing bacteria.

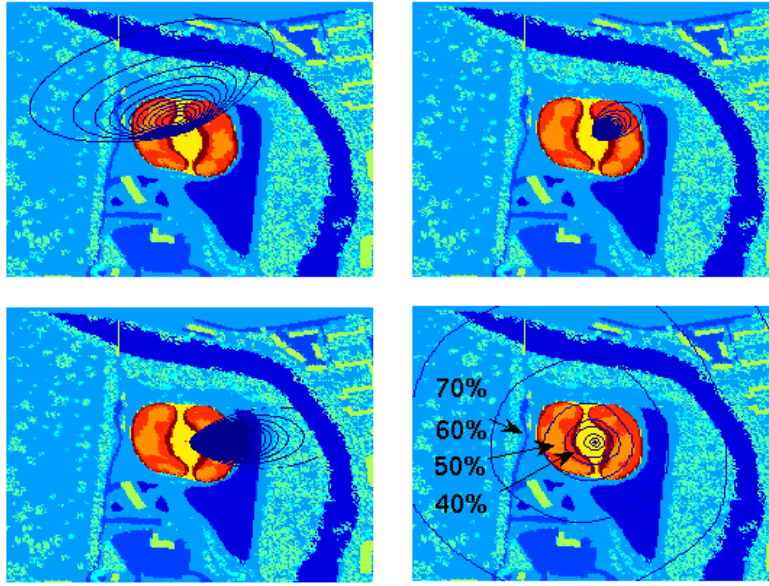


Figure 1. Footprint illustrations. The footprint probability is plotted using blue contour lines. The microsites of the wetland area are mapped using different colors. Orange marks the open water in the research wetlands. Red marks the macrophyte area. Yellow marks the upland forest area between the two wetlands. These three microsites compose the target wetland area. Grass, trees, and other water areas (river, vernal pools and ponds) are marked in shades of blue. Buildings are green. A) Example of a footprint that indicates that the flux data mostly originated from grass, trees and the river areas outside the research wetlands and therefore the data for this specific half hour should be trimmed. This data were collected when the boundary layer was stable. B) Example of a period when the probability of the signal originating from the wetland was larger than 90%. C) An example for a borderline acceptable period when wetland footprint probability was only slightly higher than 34%. D) The 2-year overall flux footprint. More than 50% of the signal originates from the wetlands and the wind distribution lead to more or less circular symmetric footprint around the wetland area.

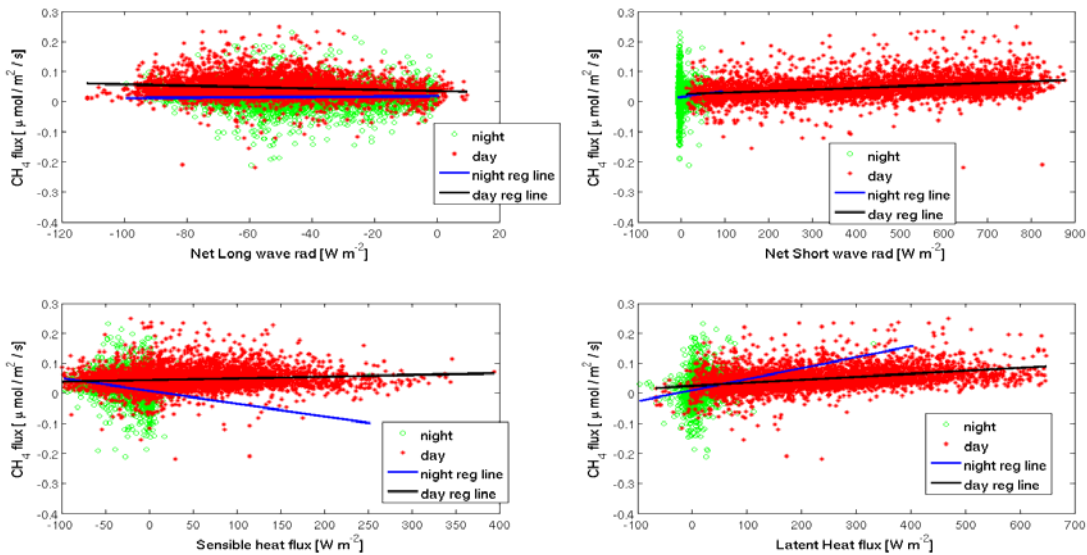


Figure 2: Drivers Vs. CH_4 flux, Summer 2011/03 to 2013/03. The effects of longwave and shortwave radiation and of sensible and latent heat fluxes. Figure 3: Drivers Vs. CH_4 flux. The effects of air temperature, Vapor pressure deficit (VPD, a combined measure of air humidity).

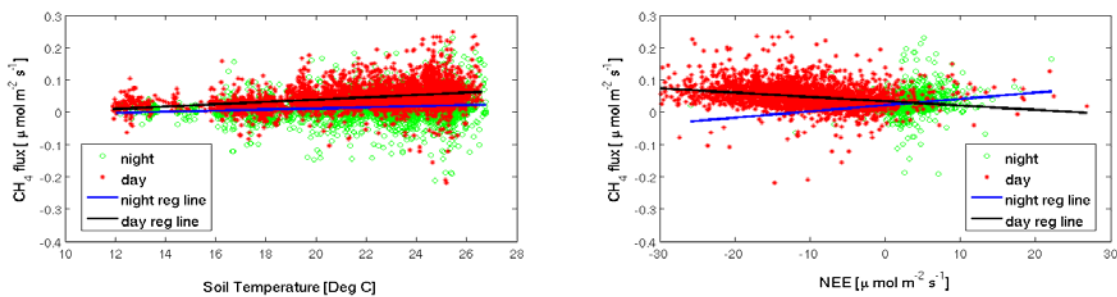


Figure 3: Drivers Vs. CH₄ flux. The effects of soil temperature and net ecosystem carbon exchange (NEE).

Significance

Our findings suggest that a range of physical and biotic conditions affect methane emission rates. Different management strategies may be developed to control the physical conditions (water temperature and heat flux for example could be reduced by trees that shade the water). Macrophyte plants, such as cattails play a critical role in transport and production of methane and provide one of the imported controls to methane emission rates.

Publications/Conference Presentations (since 3/2012)

Publications

1. Bohrer G, Zhu K, Jones RL, Curtis PS. (2013) Optimizing wind power generation while minimizing wildlife impacts in an urban area. Plos One 8:e56036.
2. Barr AG, Richardson AD, Hollinger DY, Papale D, Arain MA, Black TA, Bohrer G, Dragoni D, Fischer ML, Gu L, Law BE, Margolis HA, McCaughey JH, Munger JW, Oechel W, Schaeffer K. (2013) Use of change-point detection for friction-velocity threshold evaluation in eddy-covariance studies. Agricultural & Forest Meteorology 171:31-45.

Conference presentations

1. Mouser, PJ, Brooker, M, Mitsch, W, and Bohrer, G. 5/2012, Factors Influencing Microbial Gas Production Rates in a Constructed Wetland Ecosystem. Oral Presentation, 30th AMS Conference on Agricultural and Forest Meteorology, Boston, MA.
2. Bohrer, G, Naor-Azieli, L, Mesi, S, Mouser, PJ, Stefanik, K, Schafer, KVR, and Mitsch, W 5/2012, Determining the meteorological forcing that affect seasonal and diurnal dynamics of methane emissions at a constructed urban wetland in Ohio. Oral Presentation, 30th AMS Conference on Agricultural and Forest Meteorology, Boston, MA.
3. Bohrer G, Naor-Azieli L, Mesi S, Schäfer KVR, Mouser P, Stefanik K, Mitsch WJ, Morin T. 10/2012. Eddy flux measurements of methane at the Oletangy River Wetland Research Park wetland - Determining the seasonal and diurnal dynamics of methane emissions. Oral presentation, 4th International EcoSummit on Ecological Sustainability, Columbus, OH.

4. Mouser P, Brooker M, Bohrer G. 10/2012. Factors influencing microbial gas production rates in wetland sediments. Oral presentation, *4th International EcoSummit on Ecological Sustainability*, Columbus, OH.
5. Schäfer KVR, Bohrer G. 10/2012. Effect of restoration on the carbon balance in the Meadowlands of New Jersey. *4th International EcoSummit on Ecological Sustainability*, Columbus, OH.
6. Schäfer KVR, Bohrer G, Reid M, Tripathee R, Jaffe P. 10/2012. Temporal and spatial dynamics of methane fluxes in a temperate urban wetland. Oral presentation, *4th International EcoSummit on Ecological Sustainability*, Columbus, OH.
7. Schäfer KVR, Bohrer G, Tripathee R. 4/2012. Carbon sequestration by *Phragmites australis*. *Northeast Natural History Conference 2012*, Syracuse, NY.
8. Bohrer G, Morin T, Naor-Azrieli L, Mouser PJ, Mitsch WJ, Schafer KVR. 12/2012. Determining the meteorological forcing that affect seasonal and diurnal dynamics of respiration and GPP in a constructed urban wetland in Ohio. Oral Presentation. *American Geophysical Union Meeting 2012*, San Francisco, CA.
9. Brooker M, Bohrer G, Mouser PJ. 12/2012. Factors Influencing Microbial Carbon Emission Potential from Wetland Sediments and its Relation to Surface- and Plot-Scale Measurements. Poster, *American Geophysical Union Meeting 2012*, San Francisco, CA.
10. Schafer KVR, Tripathee R, Bohrer G. 12/2012. Effect of restoration on carbon fluxes in urban temperate wetlands. Poster, *American Geophysical Union Meeting 2012*, San Francisco, CA.
11. Morin T, Bohrer G, Naor-Azrieli L, Mesi S, Schafer KVR, Stefanik K, Mitsch WJ. 11/2012. Effects of environmental conditions on an urban wetland's methane fluxes. Poster, *41st Annual Water Management Association of Ohio Conference*, Columbus, OH.
12. Brooker M, Mouser PJ, Bohrer G. 9/2012. Quantifying in situ rates of methanogenesis and denitrification in wetland sediments. Poster, *4th International EcoSummit on Ecological Sustainability*, Columbus, OH.
13. Scannell GS, Bohrer G, Jones RL. 9/2012. Green solutions for wet weather management. Poster, *4th International EcoSummit on Ecological Sustainability*, Columbus, OH.
14. Brooker MR, Bohrer G, Mitsch WJ, Mouser PJ. 7/2012. Factors influencing methane emission potential from wetland sediments. Poster, *Ohio River Basin Consortium for Research and Education 2012*, Athens, OH.
15. Mesi S, Bohrer G, Naor-Azrieli L, Brooker M, Mouser P. 6/2012. Spatial-temporal intermittency of methane flux in an urban temperate wetland. Poster, *12th Annual American Ecological Engineering Society Meeting*, Syracuse, NY.

Students Supported By Project

Two students worked on the project but none received direct support during the first project year

- 1) Liel Naor-Azrieli – M.S. student in Environmental Science Graduate Program (Support from the ESGP as a GTA).
- 2) Timothy Morin – Ph. D. student in Environmental Science Graduate Program (Support from the OSU Graduate School as a University Fellow).

Awards or Achievements

None to date.

Discriminating Biotic and Abiotic Arsenic Release Processes under Highly Reduced Ground Water Conditions

Basic Information

Title:	Discriminating Biotic and Abiotic Arsenic Release Processes under Highly Reduced Ground Water Conditions
Project Number:	2012OH262B
Start Date:	3/1/2012
End Date:	5/31/2013
Funding Source:	104B
Congressional District:	15
Research Category:	Water Quality
Focus Category:	Geochemical Processes, Toxic Substances, Water Quality
Descriptors:	
Principal Investigators:	John Lenhart, Paula J Mouser

Publication

1. Stuckman, M.Y., Lenhart, J.J., Mouser, P.J. and Z. Zheng, 2013, "Biotic and Abiotic Release Processes from Groundwater Aquifers under Methanogenic and Transient Redox Conditions", Presented at the 245th ACS National Meeting, New Orleans, LA.

Discriminating Biotic and Abiotic Arsenic Release Processes under Highly Reduced Ground Water Conditions

2013 Annual Report

John J. Lenhart, Ph.D. and Paula J. Mouser, Ph.D., P.E.
Department of Civil, Environmental and Geodetic Engineering
The Ohio State University
Columbus, Ohio 43210

Statement of Critical Regional or State Water Problem

Ground water is important to the residents of Ohio, with approximately 76% of the community water systems, over 99% of the non-community water systems, and nearly 1 million rural homes utilizing ground water. In total, approximately 4.5 million residents of Ohio, or roughly 40% of the population, depend upon ground water as their source for drinking water. In Ohio ground water, arsenic is the contaminant that most frequently exceeds a health-related drinking-water standard with approximately 17% of the public supply wells producing water that exceeds the Maximum Contaminant Level of 10 $\mu\text{g/L}$. Unfortunately, domestic wells are not routinely tested for arsenic, so most well owners do not know whether their water has elevated concentrations. As a general trend, ground water arsenic concentrations in Ohio are relatively insensitive to the amount of arsenic in the aquifer solids and are instead sensitive to the redox state of the aquifer.

Since ground water concentrations of arsenic in Ohio are tied to the predominant redox state of the system, understanding the conditions that foster certain redox states is critical in siting an appropriate location for a drinking water well. Identifying specific processes or mechanisms responsible for inducing shifts in ground water systems from redox conditions that hinder arsenic mobilization to those that enhance arsenic mobilization is a critical component of this procedure. Details of these processes are lacking, however, and their importance in driving arsenic release in the ground waters of Ohio and elsewhere are still poorly understood. This research will evaluate how redox state changes influence arsenic release behavior. Such knowledge could be used to identify sites with conditions likely to produce arsenic release and is important for maintaining the quality of ground water that approximately five million people in Ohio depend upon for their daily needs.

Research Objective

The proposed research is driven by two overarching objectives that speak to critical knowledge gaps regarding how arsenic release in aquifer systems depends upon redox conditions. They are:

- A. Characterize mechanisms and pathways responsible for arsenic release from aquifer solids under methanogenic conditions.**
- B. Relate redox conditions and changes in arsenic release/sequestration to dominant microbial community members.**

In order to address these objectives, we propose to link detailed macroscopic-level and atomic-level characterization of chemical processes with gene-based microbial community analyses in order to elucidate details of the chemical and biological processes that drive As release and sequestration under transient redox conditions. To do so requires testing the following hypotheses.

Hypothesis A: Arsenic release under methanogenic conditions results from microbially catalyzed dissolution of residual iron oxides in the absence of sulfur or sulfide.

Hypothesis B: Redox-state dependent arsenic release patterns (see Table 1) can be reproduced by changing the concentration of dissolved organic matter in the system.

Hypothesis C: Under similar redox conditions, microbial community profiles do not differ significantly between soil depths; however, archaea species are in greater abundance under methanogenic conditions with accumulated dissolved arsenic.

Methods and Procedures

The project combines bench-scale laboratory experimental work with atomic-level spectroscopy and molecular techniques to evaluate arsenic release and sequestration under transient redox conditions. The research plan was divided into two research tasks necessary to address the proposed objectives and hypothesis. Task 1 assesses arsenic release/sequestration from iron-reducing, sulfate-reducing and methanogenic systems under ambient conditions and as influenced by transients in DOM concentration. In Task 2, we will characterize arsenic speciation in the solids under select iron-reducing, sulfate-reducing and methanogenic conditions.

Study Materials

Aquifer materials for this work were provided courtesy of Dr. Mary Ann Thomas of the USGS. These samples were collected in 2004 - 2005 from southwestern Ohio as part of an effort headed by the USGS to characterize and relate the solid-phase properties of aquifer material and ground water quality to arsenic concentrations (Thomas et al. 2008). The sample site is located in an agricultural and rural residential area thought to be free of any anthropogenic inputs of contamination. The aquifer is comprised of glacial deposits that range in depth from 35 to 120 ft. The samples were collected during the drilling of two monitoring wells as described by Thomas et al. (Thomas et al. 2008). The samples consist of primarily silty, sandy till and some sand or gravel. Transitions between glacial episodes are evident in discontinuities in the physical and chemical properties of the solids. After collection, the samples were air dried, purged with nitrogen and sealed with tape for storage (Thomas et al. 2008). The physical and chemical properties of the samples are described by Thomas et al. (Thomas et al. 2008). For this work, we restricted our analyses to samples from depths in the aquifer that correspond to iron-reducing, sulfate-reducing or methanogenic conditions. Prior to analyses the samples were ground to a uniform particle size and autoclave sterilized.

We used ground water collected directly from the site as a nutrient and microorganism inoculum in our experiments. The samples were collected in August 2012 from depths that correspond with those for the specific aquifer solids examined. These samples were collected by the PI, one

graduate student, one undergraduate student and two USGS personnel using a submersible pump. Sample pH, dissolved oxygen, temperature, oxidation-reduction potential and total dissolved solids were measured immediately in the field using a YSI 556 multiprobe system calibrated with standard solutions prior to each use. Samples were stored in zero-head space sterilized containers, placed on ice and immediately transferred to the environmental engineering laboratories at Ohio State. Aliquots of the samples were analyzed as described in the following section and the remainder was stored at 4 °C until use.

Analytical Methods

Assessment of the dissolved concentration of inorganic elements (e.g., As, Ca, Cr, Fe, K, Pb, Mg, Mn, Na, S, U, Zn) was measured using inductively coupled plasma atomic emission spectrometry (ICP-AES) or graphite furnace atomic absorption (GFAA) spectrometry. All samples were filtered through a 0.22 µm PTFE membrane prior to analyses and acidified using trace-metal grade nitric acid. Calibration was conducted using ICP grade standards (Ricca Chemicals). Anion concentrations (acetate, bromide, chloride, nitrate, nitrite, phosphate, and sulfate) were analyzed using a Dionex ICS-2100 ion chromatography (IC) with an AS19 column and bicarbonate eluent. Dissolved and total organic and inorganic carbon (DOC/TOC and DIC/TIC) was conducted using a Shimadzu TOC 5000 carbon analyzer. Nitrogen species, sulfide and phosphorus were measured with a UV/vis spectrophotometer using the hypochlorite method (ammonium), persulfate digestion (total nitrogen), methylene blue (sulfide) and molybdovanadate method (total phosphorus). Organic nitrogen (TON) were calculated as the difference between the total and inorganic nitrogen species. Arsenic speciation was evaluated using As speciation cartridges purchased from MetalSoft Center and GFAA. Iron speciation was determined using the ferrozine method as described by Hansel et al. (Hansel et al. 2003).

Specific Research Tasks

Task 1A: Evaluate and characterize arsenic release/sequestration under ambient redox conditions. A series of three experiments were conducted to investigate As release and sequestration from the aquifer solids under ambient iron-reducing, sulfate-reducing and methanogenic conditions that approximate those *in situ*. Biotic microcosm experiments were conducted by combining groundwater containing indigenous microorganisms isolated from iron-reducing, sulfate-reducing or methanogenic depths of the site with autoclave-sterilized aquifer media from the same depth into sterile serum bottles (150 ml) at approximately a 2:1 ratio. The serum bottle liquid, media, and headspace were gassed with 80:20% N₂:CO₂, sealed with rubber septa, and crimped closed to maintain anaerobic conditions. Bottles were incubated at 30°C for several weeks in the dark. Biogeochemical changes in the systems were tracked by periodically extracting samples to evaluate solution chemistry and microbial community dynamics throughout the experiment. Abiotic experiments were conducted as described for biotic treatments, with the exception that in addition to the aquifer media being sterilized, the fluids were also be autoclave-sterilized of biological organisms.

Periods of rapid change in solution biogeochemistry in these experiments was used as a guide for selecting samples for profiling the microbial community. Nucleic acids for microbial community analysis were extracted using the PowerSoil DNA Isolation Kit (MoBio Labs, Carlsbad, CA). Dynamics were assessed using bacterial and archaeal primers targeting the 16S rRNA gene. Profiles were created using terminal restriction fragment length polymorphism (T-RFLP) by

labeling the forward primer with a fluorescein dye and digesting with restriction enzymes as described by (Mouser et al. 2010). Electropherogram analysis was conducted using Genemapper and T-REX software. For sequencing of the 16S rRNA gene, unlabeled PCR products were cloned into the TOPO TA vector and chemically competent *E. coli* cells (Invitrogen, Carlsbad, CA). Key inserts from 96 clones identified during fragment analysis and cloning were amplified with the M13F primer and purified for sequence analysis at OSU's Plant-Microbe Genomics Facility. Key sequences were compared to closest known relatives in the NCBI GenBank database, to elucidate species phylogeny and possible function in the systems.

Task 1B: Evaluate and characterize arsenic release/sequestration under transient conditions.

Experiments evaluating system behavior in response to changes in DOM concentration were conducted as described in Task 1A for the ambient systems. The DOM amendments were comprised of (a) DOM concentrated from approximately 5 L of groundwater after first removing suspended solids and microbial cells (0.22 glass fiber filter) and (b) 10 mM sodium acetate. The DOM was concentrated on a reversed-phase silica SPE Bond Elut C18 column (Agilent Technologies). Concentrations tested varied across a similar range to those observed in these aquifer systems. Each of these experiments was conducted in triplicate and the solution phase chemistry and community structure analyses followed methods previously described.

Task 2: Investigate solid-state As speciation under specific redox conditions. Samples were collected from select experiments in Task 1 for analyses using x-ray absorption spectroscopy (XAS) at Argonne National Laboratory in Argonne, IL in order to identify the predominant As oxidation state and structure. Identification of oxidation state will depend upon analyses of the x-ray absorption near edge structure (XANES), whereas structural analyses will rely on computational fits to the extended x-ray adsorption fine structure (EXAFS). Both of these require analyses using proper standards. The XAS sample preparation, data collection and model fits will follow methods described in (Stuckman et al. 2012).

Progress Summary

Work over the past year comprised much of that listed under Task 1, with samples needed for Task 2 analyses also collected and currently being stored for future analyses.

Principal Findings

A series of batch microcosm experiments were conducted with the solids and ground water from the three redox zones: iron-reducing, sulfate-reducing, and methanogenic. At the same time a parallel set of experiments was conducted using DOM-amended microcosms. In both cases, very little activity was observed, indicating the levels of carbon were not sufficient to spur microbial growth (data not shown). The microcosms were subsequently amended with 10 mM sodium acetate and allowed to equilibrate for several weeks. The results of these experiments are still being analyzed and interpreted and thus will those results collected for the iron reducing systems (Site A) will be described here.

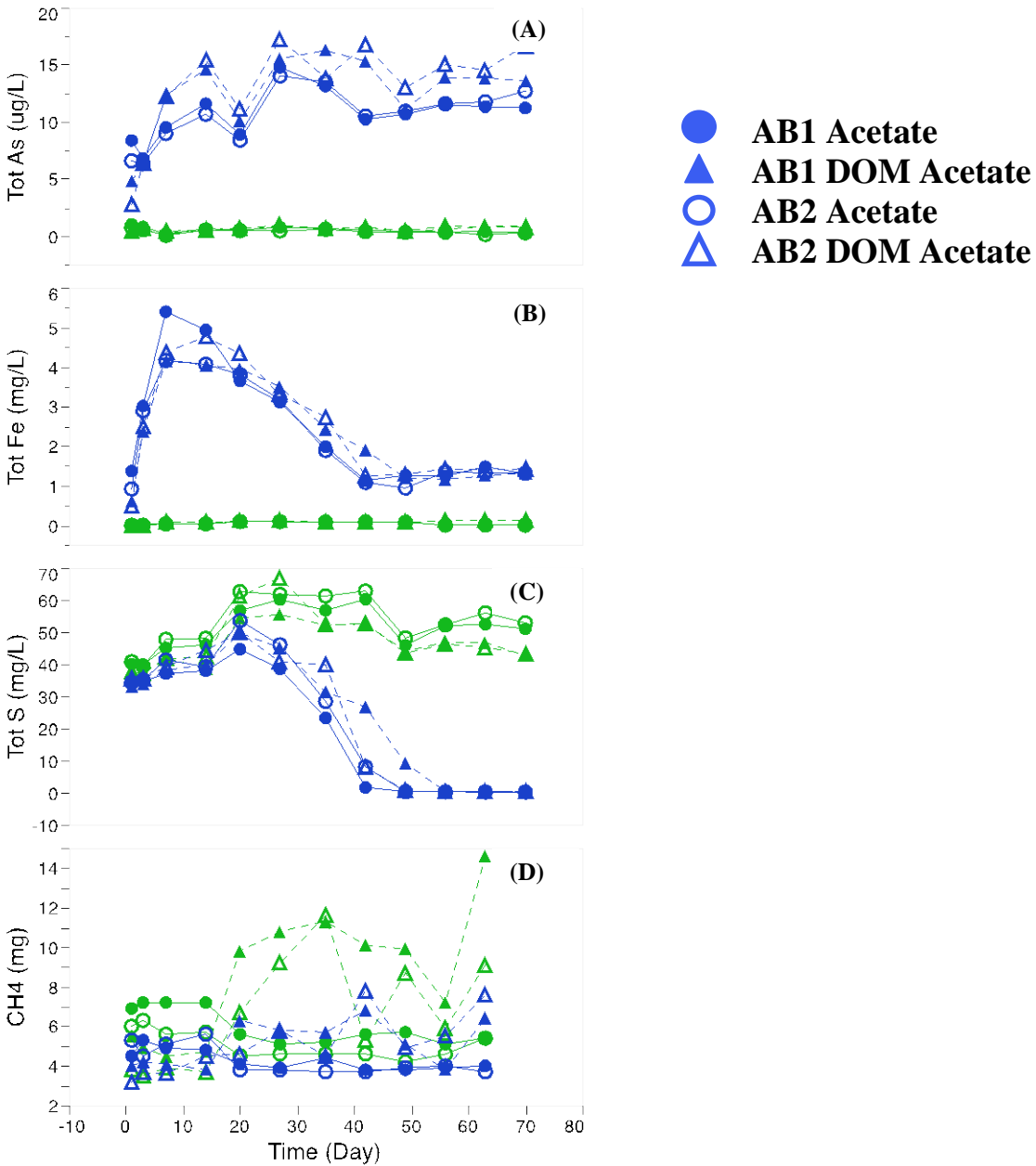


Figure 1 – Concentrations of (A) total arsenic, (B), total iron, (C), total sulfur, and (D) methane released during the incubation of ground water and sediments from iron reducing aquifer. Results are presented for duplicate samples amended with 10 mM sodium acetate (closed symbols) or 10 mM sodium acetate plus additional native DOM (open symbols). The green symbols were for abiotic controls.

Over the course of the study, concentrations of total arsenic were observed to roughly double (Figure 1A) from an initial concentration of approximately 5 ppb to 10 ppb. Most of this increase occurred over the first forty days and coincided with the rapid increase and subsequent

decline in iron (Figure 2B) as well as a decrease in total sulfur (Figure 2C). Over this time methane produced was observed to be small and near that measured for the control samples (Figure 1D). Overall these trends are consistent with release of arsenic concurrent with the reductive dissolution of iron. Similar results collected for samples from the sulfate-reducing and methanogenic aquifer layers produced results that paralleled these results indicating iron- and sulfate-reducing conditions were achieved. Additional work is being conducted to investigate release trends between iron and arsenic for the two systems to better identify potential mechanisms and processes.

Analyses of microbiological community structure (data not shown) in the systems noted that initial communities for the iron-reducing and sulfate-reducing systems were very similar. Upon spurring growth with the addition of acetate, however, both systems converged to have very similar community structures.

Future work consists of (1) correlating release of arsenic and other elements to specific pathways denoted by the presence of particular microorganisms and (2) evaluating sulfur, iron and arsenic speciation in the sediments pre- and post-incubation.

Publications

Stuckman, M.Y., Lenhart, J.J., Mouser, P.J. and Z. Zheng, 2013, "Biotic and Abiotic Release Processes from Groundwater Aquifers under Methanogenic and Transient Redox Conditions", Presented at the 245th ACS National Meeting, New Orleans, LA.

Students Supported

Mengling Stuckman (Ph.D. student in the Environmental Science Graduate Program at The Ohio State University)

Awards or Achievements

None at this time.

References cited

- Hansel, C. M., et al. (2003). "Secondary mineralization pathways induced by dissimilatory iron reduction of ferrihydrite under advective flow." Geochimica et Cosmochimica Acta **67**(16): 2977-2992.
- Mouser, P. J., et al. (2010). "Enhanced detection of groundwater contamination from a leaking waste disposal site by microbial community profiles." Water Resources Research **46**.
- Stuckman, M. Y., et al. (2012). "Evaluating the Release of Arsenic from Drinking Water Absorbents under Regulatory and Landfill Leaching Conditions Using X-ray Adsorption Fine Structure (XAFS) Spectroscopy." Environmental Science & Technology **In Review**.
- Thomas, M. A., et al. (2008). Relation Between Solid-Phase and Dissolved Arsenic in the Ground-Water System Underlying Northern Preble County, Ohio, United States Geological Society.

An Integrated Framework for Response Actions for a Drinking Water Distribution Security Network

Basic Information

Title:	An Integrated Framework for Response Actions for a Drinking Water Distribution Security Network
Project Number:	2012OH311O
Start Date:	8/1/2012
End Date:	7/31/2013
Funding Source:	Other
Congressional District:	1
Research Category:	Engineering
Focus Category:	Management and Planning, Solute Transport, Models
Descriptors:	
Principal Investigators:	Dominic L Boccelli

Publication

1. Rana, M. and Boccelli, D. L. (2013). "Contamination Spread Forecasting and Identification of Sampling Locations in a Water Distribution Network." World Water and Environmental Resources Congress, ASCE, Cincinnati, OH. [oral presentation]

An Integrated Framework for Response Actions for a Drinking Water Distribution Security Network

Problem and Research Objectives

The use of non-specific water quality sensors have provided the foundation for developing contamination warning systems (CWS) for drinking water distribution systems to protect public health from (un)intentional intrusion events. These non-specific water quality sensors (e.g., chlorine, pH, conductivity, etc.) can be linked with data driven event detection algorithms to determine when anomalous water quality conditions occur. The ability to detect water quality events has led to the development of forensic tools, such as contaminant source identification, and response strategies to mitigate the impact on the population. However, there has been little activity associated with translating the CWS signals and contaminant source information into predicting the future transport of a contamination event to inform response activities. Thus, there is a critical need to develop an integrative framework that can propagate the impacts of contaminant source uncertainty through distribution system transport to provide more information for utilizing response tools. The objective of this project, which is the next step towards developing an integrated real-time security application, is to develop a framework that will forecast contaminant spread throughout the distribution system based on the current estimated state of potential contaminant sources, which will then be utilized to inform confirmatory sampling locations to improve our estimates of contaminant spread and source location.

Methodology

Our central hypothesis is that contaminant source identification algorithms can be utilized to assess the potential contaminant spread, and provide needed information to select confirmatory sampling locations to improve our estimates of contaminant source identification and spatial distribution of an event. The rationale for developing this framework is to better utilize the information generated via CWS for assessing the overall impact throughout the distribution system and provide more appropriate response actions. We will test our central hypothesis and associated objectives by pursuing the following: 1) implement a forecasting algorithm to propagate probabilistic information associated with potential contaminant source locations to assess contaminant spread; 2) develop an approach for identifying confirmatory sampling locations that seeks to maximize new information associated with a contamination event; and 3) create an output format conducive for visualization purposes.

Forecasting Algorithm. For a given sensor network design, the forecasting algorithm will rely on the PCSI algorithm of Yang and Boccelli (2013) and the EPANET distribution system modeling software (Rossman, 2000) – to identify and characterize the probability of a specific location as a potential contaminant source. As sensors report positive or negative alarms (i.e., indicating an event has occurred or safe conditions exist, respectively), the PCSI algorithm utilizes the backtracking algorithm (Shang et al., 2002) to determine the upstream location-time pairs that are hydraulically connected to the observed sensor signal. Then, a Bayesian updating procedure – a Beta-Binomial conjugate pair – is used to update the probability that the location-time pair was the source (a positive alarm increases the probability; a negative alarm decreases the probability). For large networks, the PCSI algorithm will identify multiple potential source locations. The backtracking algorithm, in conjunction with hydraulic information, will be used to efficiently forecast the short-term (e.g., up to 6 hours) spread of contaminant from the individual sources represented as a “conservative tracer.” For each of the downstream nodes, the flow-weighted probabilities from the potential source locations will be assumed to characterize the probability of a contaminant being at the downstream location.

Identifying Confirmatory Sampling Locations. The following sections first identify the metric used to quantify the information associated with sampling locations, and then how the best sampling location is determined.

Entropy as Information. Within the area of Information Theory, “entropy” is provided as a metric of information – more specifically, entropy represents the average information contained within a specific distribution (Reza, 1961). For example, if we are provided a discrete distribution of n classes, where each class has an associated probability p_i , $\sum p_i = 1$, the entropy of that distribution is defined as

$$H(P) = - \sum_{i=1}^n p_i \log_2 p_i$$

where P represents the overall distribution and $H(P)$ the expected information, or entropy, contained within that distribution. For a uniform distribution (i.e., p_i is the same for all classes), $H(P)$ has maximum entropy defined as $\log_2(n)$. When we have perfect information regarding one class (i.e., $p_i = 1$, $p_j = 0$ when $i \neq j$) then $H(P)$ has a minimum entropy of 0. Thus, decreasing entropy represents increased information associated with the discrete distribution.

Confirmatory Sampling Selection. The intent behind confirmatory sampling is to increase the information associated with the potential source or forecasted locations. The initial entropy estimates for the potential source and contaminant spread locations can be estimated using the probabilities developed from the PCSI algorithm. To determine the amount of information gained (or lost) by confirmatory sampling, we need to perform the following steps for each potential sampling location: i) identify the probability that the sampling location could result in a contaminant observation; ii) assume that the resulting confirmatory sample returned a positive or negative alarm and separately update the PCSI results; iii) for each set of updated source probabilities, update the probabilities of the forecasted contaminant spread; iv) calculate the updated entropies for the source and forecasted locations assuming both positive and negative alarms; and v) use the probability value associated with observing the contamination event at the sampling location (from step i) to calculate the expected entropies for the source and forecasted locations based on the updated entropies from step iv. The differences between the initial and updated entropies represent the expected amount of information gained (or lost) by performing confirmatory sampling at that individual location. Confirmatory samples with the largest information differences indicate the locations that would provide the most new information.

The benefit to this approach is that an increase in information can occur by either selecting locations that would reinforce higher probability source locations, or, vice-versa, that would reinforce lower probability source locations. In either case, the overall information would be increased by generating a distribution such that the probability of the most likely candidate location(s) also increased. Computationally, this approach is also attractive because updating the probabilities is relatively straightforward since all of the necessary hydraulic and water quality simulations have been performed leaving only the algebraic calculations to update the probabilities. The relative ease of computation will allow an enumeration approach to be utilized to identify confirmatory sampling locations rather than using a formalized optimization algorithm (e.g., a mixed-integer non-linear programming approach) that would likely be more computationally intensive.

Principal Findings and Significance

In order to test and evaluate the forecasting and sampling algorithm, a test network (the Net 3 example included with EPANET) was utilized. Figure 1 presents the network model as well as the placement of five water quality sensor locations (blue symbols). A 1-hour contaminant injection was simulated at node 10 starting at the 3rd hour of the simulation. The first detection of the contaminant occurs at the 5th hour at the water quality sensors located at Node 193.

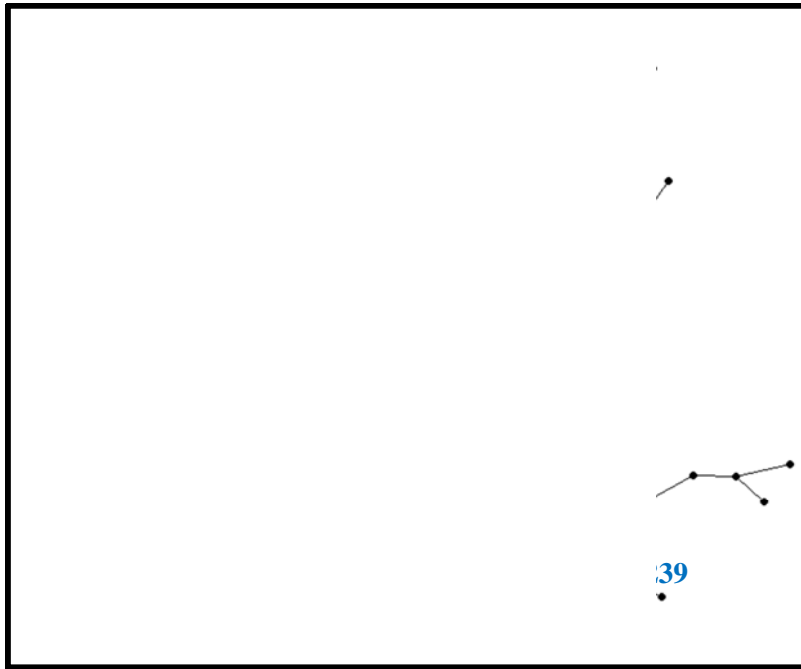


Figure 1. Example network for testing the forecasting and sampling algorithm.

Once the contaminant reaches a water quality sensor, the detection of the contaminant along with the hydraulics can be utilized with the PCSI algorithm to determine the probabilities of the upstream nodes. Figure 2 presents the upstream locations that have probabilities of greater than [red] or less than [green] a 50% probability of being a source, as determined by the PCSI algorithm.

Figure 3 [top] shows the forecasted change in entropy for all of the 97 possible sampling locations; a line plot (instead of a scatter plot) is used to more clearly show the results [the Node Index is an internal EPANET variable; the Node ID shown in the graph is the identifier of the actual location]. The peaks within each box are associated with the Node ID value provided, and represent the larger changes in entropy (remember, decreasing entropy suggests more information). For Nodes 1 (the biggest change), 40, and 179, these locations are either the tank or associated with the pipe to/from the tank. Node 237 is potentially downstream of contamination spread. In addition to Node 237, Nodes 206, 208, 209, 211, and 213 all have similar drops in entropy as these are all hydraulically “close” to Node 237.

Figure 4 [top] shows the resulting change in entropy for all of the 97 possible sampling locations *after* the simulation is moved ahead one hour; a line plot is used to more clearly show the results [the Node



Figure 2. Estimated source probabilities at hour 5 of the simulation; red symbols represent locations with probabilities of being a source greater than 50%, green symbols represent locations with probabilities of being a source greater than 50%.

Index is an internal EPANET variable; the Node ID shown in the graph is the identifier of the actual location]. These results provide information associated with the “true” information of the system at the next hour. The peaks within each box are associated with the Node ID value provided, and represent the larger changes in entropy (remember, decreasing entropy suggests more information). The nodes near the tank (1, 40, 179 and 271) would have provided the greatest decrease in information. The approach correctly identified Node 1 as the best sampling location and, with the exception of Node 271, also identified Nodes 40 and 179 as sampling locations with more significant decreases in entropy (Figure 3). Additionally, Nodes 199, 201 and 202, which are just downstream of Tank 1, also appear to be significant during the next hour. For the forecasted sampling, Nodes 206, 208, 209, 211, 213, and 237 were all shown to have similar impacts on entropy (Figure 3). While Nodes 211, 213 and 237 show a slightly less drop in “actual” entropy relative to the forecasted entropy, these locations were still identified. However, Nodes 206, 208 and 209 did not appear to have as significant an impact on entropy as forecasted, but Node 241 appears to have been a good place to sample that was not one of the higher locations identified in the forecasting portion of the algorithm.

The contribution of this research is significant as this study effectively bridges the gap between the information generated from a contaminant warning system (via sensor response and contaminant source identification) and the initial phases of response (via confirmatory sampling). These results will provide the foundation for developing more robust response activities when attempting to mitigate the impact of an intrusion event.



Figure 3. Plots of the forecasted change in entropy for each potential sampling location [top], as well as the spatial location of the sampling nodes that result in the greatest decrease in entropy (i.e., largest increase in information).

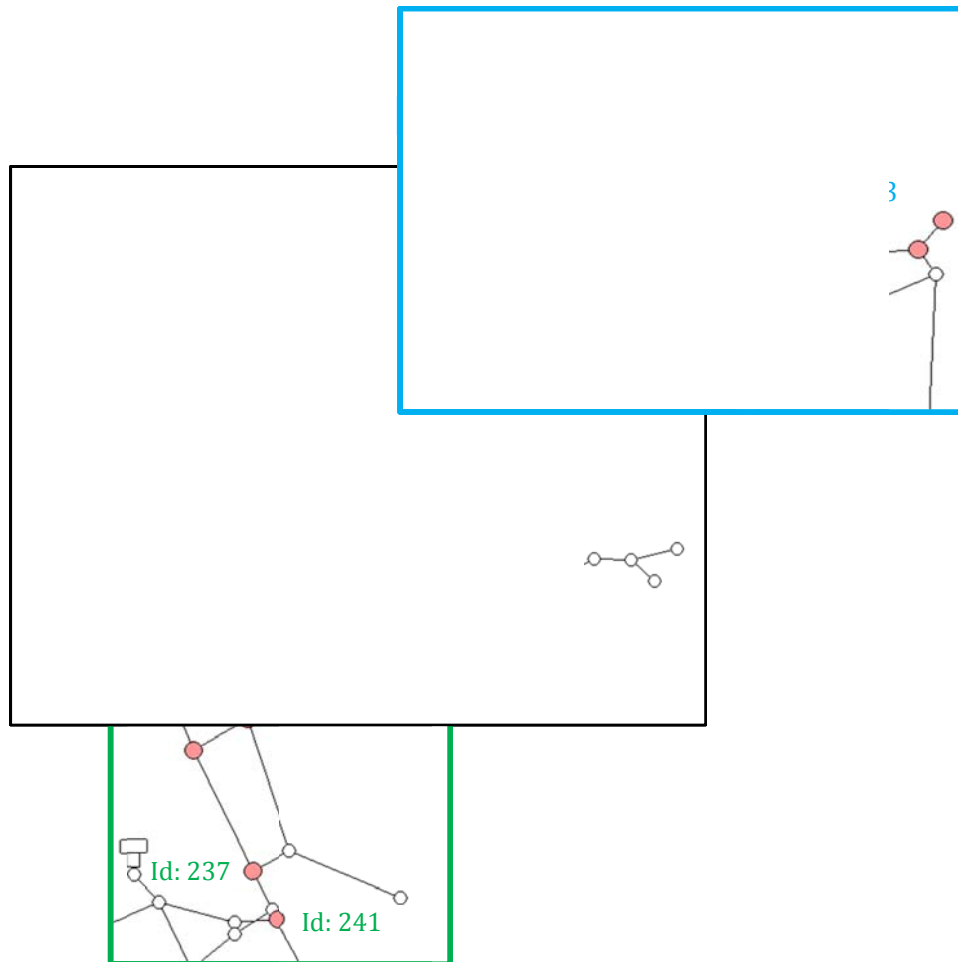
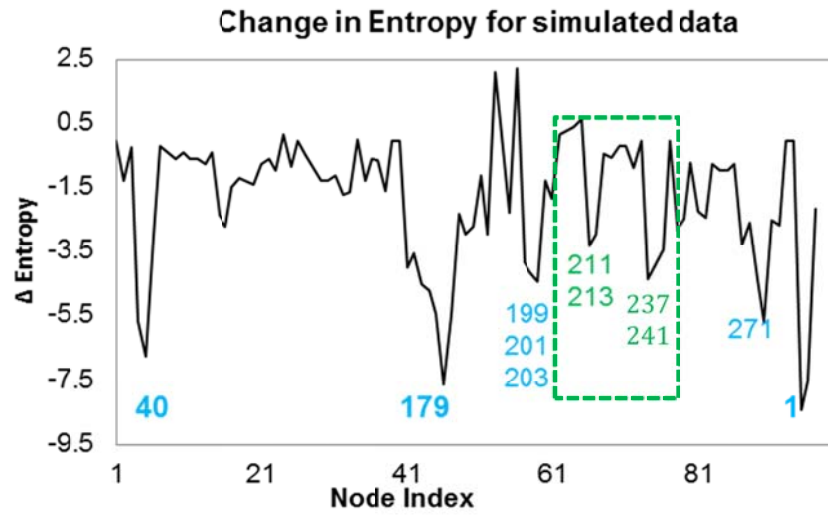


Figure 4. Plots of the forecasted change in entropy for each potential sampling location [top], as well as the spatial location of the sampling nodes that result in the greatest decrease in entropy (i.e., largest increase in information).

Publication Citations

Rana, M. and Boccelli, D. L. (2013). "Contamination Spread Forecasting and Identification of Sampling Locations in a Water Distribution Network." *World Water and Environmental Resources Congress, ASCE*, Cincinnati, OH. [oral presentation]

Number of Students Supported

The research has funded one MS student (Masud Rana) in Environmental Engineering.

Awards or Achievements

N/A

Professional Placement of Graduates

N/A (Mr. Rana is still working on his MS degree.)

References

Reza, F. M. (1961) *An Introduction to Information Theory*. McGraw-Hill, New York.

Rossman, L. A. (2000) *EPANET2 User's Manual*. Cincinnati, OH: Risk Reduction Engineering Laboratory, U.S. Environmental Protection Agency.

Shang, F., Uber, J. G., and Polycarpou, M. M. (2002) "Particle Backtracking Algorithm for Water Distribution System Analysis." *Journal of Environmental Engineering*, 128(5), 441-450.

Yang, X. and Boccelli, D. L. (2013) "A Bayesian Approach for Real-Time Probabilistic Contaminant Source Identification." *Journal of Water Resources Planning and Management*, (under review).

Information Transfer Program Introduction

The Ohio Water Resources Center (Ohio WRC), at the Ohio State University, conducted a number of activities to transfer water related information to a wide range of state, federal, county, and municipal agencies, to the academic community, students, and to private citizens throughout Ohio. Specific activities included:

- 1) Preparation of information for the website of the Ohio WRC and maintenance of the website
- 2) Administration of a Special Water and Wastewater Treatment Grants Competition funded through the Ohio Water Development Authority - administration of the 104(B) In-State Competition and the 104(G) National Competitive Grants Program - encouraged investigators of projects funded through the Ohio WRC to develop publications in peer-reviewed journals and other outlets
- 3) Continued administrative support for the Water Management Association of Ohio (WMAO) and associated WMAO meetings, conferences, and division activities. Co-organized quarterly Ohio WRC-WMAO luncheon seminars.
- 4) Arranging and helping investigators of supported projects to disseminate their results in different newsletters published in the State of Ohio, such as Twine Line, Water Table and Buckeye Bulletin.
- 5) Assisting in organizing Ohio River Basin Consortium for Research and Education conference in Athens, Ohio and leading the water and energy session.
- 6) Responding to questions from the public regarding water resources issues in the State of Ohio.
- 7) Creating a statewide database of water related investigators in Ohio universities and sorting their research interests.
- 8) Hosted and organized joint Ohio WRC-USGS mini-symposium to engender researcher partnerships between Ohio State University and USGS Ohio Water Science Center researchers.
- 9) Led the Ohio State University Shale Water Management Network faculty group to promote research surrounding water impacts as a result of shale gas exploration and production activities.
- 10) Participated in the 2013 Central Ohio Children's Water Festival.

USGS Summer Intern Program

None.

Student Support					
Category	Section 104 Base Grant	Section 104 NCGP Award	NIWR-USGS Internship	Supplemental Awards	Total
Undergraduate	3	0	0	0	3
Masters	7	0	0	0	7
Ph.D.	5	0	0	0	5
Post-Doc.	0	0	0	0	0
Total	15	0	0	0	15

Notable Awards and Achievements

1.2011OH208B (“High-performance porous polybenzimidazole membranes for water treatment using forward osmosis”) Faculty (Isabel Escobar) Award: 2011 American Institute of Chemical Engineers (AIChE) Separations Division FRI/John G. Kunesh Award: recognizes outstanding contributions to the academic, scientific, technological, industrial, or service areas involving separations technologies for individuals under the age of 40. Criteria considered in selecting an awardee include: Significant discoveries, important research, development of new processes and products, introduction of new education concepts, service to the Separations Division, or outstanding service to the separations community.

2.2011OH208B (“High-performance porous polybenzimidazole membranes for water treatment using forward osmosis”) Student (Michael Flanagan) Award: Winner of 2012 University of Toledo, College of Engineering Outstanding MS Thesis Award.